Archives of Biochemistry and Biophysics 786 (2026) 111008

Contents lists available at ScienceDirect

Archives of Biochemistry and Biophysics

journal homepage: www.elsevier.com/locate/yabbi

Oxygen-dependent regulation of ion fluxes and intracellular pH in *Saccharomyces cerevisiae* exposed to acetic acid

Gohar Azbekyan [a,b,c], Anahit Shirvanyan [a,b,c], Nicoletta Guaragnella [d,*], Rodrigo Ledesma-Amaro [e], Karen Trchounian [a,b,c,**]

[a] Scientific-Research Institute of Biology, Faculty of Biology, Yerevan State University, 1 Alex Manoogian, Yerevan, RA, 0025, Armenia
[b] Department of Biochemistry, Microbiology and Biotechnology, Faculty of Biology, Yerevan State University, 1 Alex Manoogian, Yerevan, RA, 0025, Armenia
[c] Microbial Biotechnologies and Biofuel Innovation Center, Yerevan State University, 1 Alex Manoogian, Yerevan, RA, 0025, Armenia
[d] Department of Biosciences, Biotechnology and Environment, University of Bari Aldo Moro, Piazza Umberto 1, Bari, Italy
[e] Imperial College Centre for Engineering Biology, Bezos Centre for Sustainable Protein, Microbial Food Hub, Department of Bioengineering, Imperial College London, UK

ARTICLE INFO

Keywords:
Yeast
Acetic acid stress
Oxygen availability
Ion homeostasis
Intracellular ATP

ABSTRACT

The study of acetic acid (AA) stress in yeast is crucial for understanding the mechanisms of acid stress tolerance and enhancing production efficiency. Although AA toxicity has been extensively studied, the mechanism by which oxygen availability modulates ion flux balance and intracellular proton handling under AA stress remains poorly understood. Here, we investigated the combined effects of AA concentration, acidic pH, and oxygen availability on plasma membrane Na^+, K^+, and H^+ fluxes, intracellular pH, and growth in two *Saccharomyces cerevisiae* strains with distinct AA tolerance. We show that AA toxicity is strongly concentration-, strain-, and oxygen-dependent. AA exposure increased DCCD-sensitive proton (J_H^+) and sodium (J_{Na}^+) fluxes while progressively impairing potassium uptake (J_K^+), resulting in nonlinear, strain-specific shifts in Na^+/H^+ and K^+/H^+ exchange ratios and a substantial increase in ion exchange imbalance. These effects were amplified under oxygen-limited conditions and correlated with reduced growth and metabolic activity. Moderate AA stress was accompanied by increased intracellular ATP, particularly in ATCC 9804 under oxygen limitation, whereas severe AA stress caused ATP depletion, most strongly in ATCC 13007. Notably, the more tolerant strain maintained lower intracellular proton accumulation and more efficient ion flux coordination, particularly during aerobic growth. Together, our findings demonstrate that oxygen availability fundamentally reshapes ion flux balance and intracellular pH homeostasis during AA stress. These insights have direct implications for strain selection and process optimization in industrial fermentations exposed to weak organic acid inhibition.

1. Introduction

Acetic acid (AA) has great interest in yeast research since it is produced in yeast during alcoholic fermentation, as well as in the processing of lignocellulosic biomass [1,2]. During alcoholic fermentation, *Saccharomyces cerevisiae* generates low concentrations of AA (0.1–0.3 g L^{-1}). However, the presence of AA bacteria during wine production can increase its production, leading to undesirable effects in the fermentation process. Concentrations exceeding 0.6 g L^{-1} may already reduce the fermentation efficiency of yeast, and levels above 0.9 g L^{-1} can significantly impair the organoleptic properties of wine [1,2]. Up to 15 g L^{-1} AA can be formed during the pretreatment of lignocellulosic biomass which can have a strong inhibitory effect on the fermentation efficiency [1]. Nevertheless, AA can also be used in the food industry, together with other weak organic acids (WOS), as a natural preservative [1]. Thus, studying its effects and understanding its cellular transport, pH homeostasis, metabolism, and stress signaling pathways are important for constructing robust strains and optimization of industrial production of valuable chemicals [3].

AA can serve as a substrate for respiration in *S. cerevisiae*; however, in high concentrations, it acts as a stress factor and lead to cell death [4]. When the extracellular pH is lower than the pK_a of AA (4.76), it exists in an undissociated form that can easily diffuse across the cell membrane, depending on the molecule's solubility in the membrane [4,5]. In

* Corresponding author. Department of Biosciences, Biotechnology and Environment, University of Bari Aldo Moro, Piazza Umberto I, 70121, Bari, Italy.
** Corresponding author. Scientific Research Institute of Biology, 1 A. Manoogian street, 0025, Yerevan, Armenia.
E-mail addresses: nicoletta.guaragnella@uniba.it (N. Guaragnella), k.trchounian@ysu.am (K. Trchounian).

https://doi.org/10.1016/j.abb.2026.111008
Received 28 April 2026; Received in revised form 18 August 2026; Accepted 16 September 2026
Available online 17 September 2026
0003-9861/© 2026 The Authors. Published by Elsevier Inc. This is an open access article under the CC BY-NC-ND license (http://creativecommons.org/licenses/by-nc-nd/4.0/).

extracellular pHs exceeding the pK_a of AA, it is present mainly as acetate anions, which enter the cells through two major electroneutral proton transporters, Jen1 and Ady2 [3–5]. Hence, the effect of AA may vary depending on experimental conditions, microbial strains used, growth parameters (such as pH and medium composition), AA concentration, and duration of exposure [3].

Yeast can resist the effects of AA by remodeling the cell wall structure, restoring intracellular pH, exporting harmful anions, and other detoxification mechanisms [6]. Haa1 is a key regulator of the cellular response to AA [4]. In response to acid pH, the structure and composition of the cell wall undergo significant changes, leading to membrane deformation [7,8].

Disruptions in any of the ion gradients, specifically under stress conditions, can significantly disturb the overall electrochemical transmembrane potential and balance [9]. Despite considerable progress in studying ion fluxes and homeostasis in yeast cells, uncertainties in our understanding of intracellular ion distribution and their interactions within the cell, especially under stress conditions [9]. The plasma membrane ATPase and the vacuolar ATPase play a crucial role in regulating intracellular pH during AA stress [6]. On the other hand, Pdr12 transporter efflux acid anions via ATP-dependent mechanism, reducing their toxic effects and regulating intracellular pH [3,5,10]. However, this process leads to significant ATP consumption, reducing yeast biomass formation and growth rate. Thus, the availability and nature of carbon and nitrogen sources and minerals (K^+, Mg^{2+}, $Fe^{2+}/^{3+}$, and Zn^{2+}) and growth conditions can be determinant for yeast adaptation to AA stress [9]. Furthermore, K^+ and Na^+ ions are vital for multiple physiological processes in *S. cerevisiae*, including maintaining plasma membrane integrity, regulating cell volume, osmotic stability, compensating for negative charges of macromolecules, controlling protein synthesis, and supporting overall cellular function [9,11]. The Trk1 and Trk2 transporters maintain high-affinity K^+ influx in *S. cerevisiae*. Potassium efflux is primarily mediated by three transport systems: Nha1, Ena-ATPase, and Tok1 [12]. Nha1 actively exchanges K^+ and Na^+ ions in response to changes in acidity, helping the cell manage acid stress and maintain internal ionic balance [9].

Previous findings indicate that industrial *S. cerevisiae* strains can differ substantially in acetate production and utilization depending on oxygen availability, suggesting strain-specific metabolic adaptation strategies [13]. Despite the limited of data in the literature, it was shown that wine and beer fermentation-derived yeast strains, such as ATCC 9804 and ATCC 13007, differ by fermentation capacity, time, temperature, as well as alcohol resistance, flavor and aroma profile, nutrient requirement and flocculation properties [13–16]. The shown differences in metabolic properties, as well as previously reported differences in AA stress resistance suggest the presence of distinct adaptation mechanisms, make them a good model for understanding of strain-dependent AA responses.

The aim of this study was to determine how oxygen availability influences ion (K+; Na^+ and H^+) flux coordination and intracellular pH regulation in two *Saccharomyces cerevisiae* strains (ATCC 9804 and ATCC 13007) under AA stress. Comparing the responses of two strains with distinct AA tolerance under different growth conditions provides insight into the oxygen-dependent coordination of K^+, Na^+, and H^+ fluxes, intracellular pH, and transmembrane pH gradient regulation in response to AA, pH, and combined stresses. The data obtained contributes to elucidating the mechanisms of AA stress depending on oxygen availability, which may be useful for the development of stress-tolerant strains for the efficient bioethanol production from lignocellulosic waste material.

2. Materials and methods

2.1. Yeast and growth conditions

The *S. cerevisiae* ATCC 9804 and ATCC 13007 strains were purchased from the Microbial Depository Centre of the "Armbiotechnology" SPC of the NAS RA. *S. cerevisiae* ATCC 9804 (GenBank: Z95939.1; European archive of nucleotides (ENA): ERR5285363) was isolated from palm wine [13], and *S. cerevisiae* ATCC 13007 (prototroph, *pof+, sta,* diploid, ENA: ERR5258805) from beer [17,18]. Yeast cells were cultivated in a YPD medium (10 g L^{-1} yeast extract, 20 g L^{-1} peptone, 20 g L^{-1} D-glucose), and agar (20 g L^{-1}) was added to obtain a solid nutrient medium [19]. Medium pH was adjusted to 3.0 and 4.5 by 0.1 N HCl using an HI1131 pH-electrode combined to an HI3220 pH-ionometer (Hanna Instruments, USA). Individual colonies grown on solid medium were transferred to a liquid medium and incubated in aerobic condition at 30°C, 180 rpm [19–21]. Cells from the seed culture were transferred to a new YPD medium with final optical densities (OD) of 0.2 and were grown under aerobic (medium filling 1/3.0, with rotary shaking at 180 rpm) and oxygen-limited conditions (medium filling 1/1.2, without shaking) at 30°C (physiological condition) [22]. To examine the AA stress yeast cells were similarly cultured under aerobic or oxygen-limited conditions in YPD medium containing AA with final concentrations of 10–50 mM sterilized using a 0.22 μm sterile filter (VWR, USA) and added from stock solution (10 M) before inoculation. The specific growth rate (μ) was determined using a Cary 60 UV-Vis spectrophotometer (Agilent Technologies, Germany). The specific growth rate was calculated during the exponential growth phase as a ratio of the logarithmic difference between the optical densities doubled at 600 nm to the doubling period and expressed in h^{-1} [13,23].

2.2. Determination of extracellular redox potential, pH and osmolality

The changes in medium oxidation-reduction potential (hereafter refers as ORP), extracellular pH, and osmolality were determined during 0–168h cultivation of cells under physiological or AA stress conditions. ORP was measured using a Refillable Combination ORP electrode (HI3131, Hanna Instruments, USA) combined with HI5222 ionometer (Hanna Instruments, USA). The electrode was calibrated using control solution containing 16.13 g L^{-1} K_3 [Fe $(CN)_6$] and 21.12 g L^{-1} K_4 [Fe $(CN)_6$], the ORP was 254 ± 10 mV [24]. Extracellular pH was determined using HI1131 pH-electrode combined to an HI3220 pH-ionometer.

To determine the osmolality of the medium, 1 mL samples from 0 to 168h grown cultures were centrifuged at 8000 rpm for 10 min using Mini High Speed D2012plus Biobase Centrifuge (China). Then 100 μL of the supernatant was analyzed using a K7400-S semimicro osmometer (Knauer, Germany). The instrument was calibrated using standard solutions 300 mOsm kg^{-1} (A01240), 400 mOsm kg^{-1} (A01241-1) and 850 mOsm kg^{-1} (A01250, Knauer, Germany). The results were expressed in mOsm kg^{-1} [13,25].

2.3. Determination of ion fluxes through the whole cell plasma membrane

Mid-exponential growth phase cells were harvested using centrifugation at 3500xg for 15 min using Sorvall LYNX 6000 Ultrafast centrifuge (Thermo Scientific, USA). The cell pellet was washed twice with deionized water and centrifuged at 3160xg for 10 min at 4°C (LMC-4200R, Laboratory Refrigerated Centrifuge, Biosan, Latvia). The resulted yeast biomass was resuspended in experimental assay (150 mM Tris-PO_4 buffer containing 0.4 mM $MgSO_4$, 1 mM NaCl, and 1 mM KCl, pH 7.0). The fluxes of H^+, K^+, and Na^+ across plasma membrane were determined by the potentiometric method during the addition of glucose (20 g L^{-1}, aqueous solution). The assay was conducted in a 4.5 mL experimental assay with the final concentrations of 1.0 x 10^9 cells. Electrode readings data were outputted automatically per 10 s by LabView computer program (National Instruments Co., USA). The method relies on the principle that changes in ion concentration in the external medium reflect the net ion flux across the yeast plasma membrane [26]. Proton flux rate (J_H^+) was determined using pH-selective and reference electrodes (Hanna Instruments, USA). Potassium flux rate (J_K^+) was

measured with an HI41114 potassium-selective electrode combined with HI4114-51 module (Hanna Instruments, USA). Sodium flux rate (J^{+}_{Na}) was determined using an FC300B Na^{+}-selective electrode (Hanna Instruments, USA). The electrode readings were calibrated by titration of the experimental assay with 0.01 M HCl: 0.1 M KCl or with 0.1 M NaCl. All electrodes were connected to an HI 5222 pH/ISE/ORP-meter (Hanna Instruments, USA) [13,27]. The pH sensitivity of the sodium flux was tested with the calibration at pH 7.0-9.0 (Supplementary Fig. 1).

To understand the role of H^{+}-ATPase, cells were treated for 15 min with the 0.5 mM N, *N*′-dicyclohexylcarbodiimide (DCCD, 0.1 M stock in ethanol, specific inhibitor of H^{+}-ATPase). DCCD-sensitive ion fluxes were calculated as the difference between total ion fluxes and the corresponding fluxes measured after DCCD treatment. Positive values indicate net ion efflux, whereas negative values indicate net ion uptake. All results were expressed in mM ion min^{-1} 10^{9} CFU^{-1} [13]. The DCCD-sensitive Na^{+}/H^{+} and K^{+}/H^{+} exchange ratios were calculated from the corresponding DCCD-sensitive fluxes [13]. The ion exchange balance (Γ) was calculated as the ratio of the sum of the DCCD-sensitive Na^{+} and H^{+} effluxes to the absolute value of the DCCD-sensitive K^{+} influx.

2.4. Intracellular pH determination

Cells from 50 mL exponential growth phase culture were harvested using centrifugation at 3500xg for 15 min using Sorvall LYNX 6000 Ultrafast centrifuge (Thermo Scientific, USA). The cell pellet was washed with distilled water and centrifuged at 3160xg for 10 min at 4°C (LMC-4200R, Laboratory Refrigerated Centrifuge, Biosan, Latvia). Resulting pellets were resuspended in 2-3 mL 50 mM sodium citrate buffer (pH 3.0) and used immediately for experiments. Intracellular pH was determined using spectrofluorometer (Cary Eclipse Fluorescence Spectrometer, Agilent Technologies, USA) by monitoring the decrease in fluorescence of 9-aminoacridine upon its uptake by yeast cells with extinction at 339 nm and emission at 460 nm [28]. The dye uptake was induced by exposing 30 μL cells to 2970 μL external buffers of varying pH (100 mM Tris-HCl, pH 3.0–9.0) containing 10 nM 9-aminoacridine in 1sm quartz cuvettes. A decrease in fluorescence corresponds to increased accumulation of 9-aminoacridine inside the cells, which occurs when the external pH is higher than the intracellular pH, creating a transmembrane pH gradient that drives dye uptake. The linear curve fitting was performed by plotting the external buffer pH values against the fluorescence quenching. The intracellular pH (pH_{in}) determined from the point on the fitted curve that produced zero quenching. Transmembrane proton gradient (ΔpH) was calculated as the difference between pH_{in} and cultivation medium pH (pH_{out}) [28]. Curve fitting and calculations were carried out using Microsoft Excel 2026 and GraphPad Prism 8.0.2 software (GraphPad Software, Inc., San Diego, California, USA) [29,30].

2.5. Intracellular ATP measurement

Mid-logarithmic growth phase cells (10^{6} CFU mL^{-1}) were harvested using centrifugation at 3500xg for 10 min (LMC-4200R, Laboratory Refrigerated Centrifuge, Biosan, Latvia). Cell pellet was washed using sterile double distilled water. Intracellular ATP levels were measured using ATP assay bioluminescence kit (MAK473, Sigma Aldrich, Germany) and white opaque flat-bottom 96-well plates (Greiner Bio-One, US) by following manufacturer instructions. The method is based on the immediate reaction of released intracellular ATP followed by cell lysis and substrate, D-luciferin, in the presence of luciferase [31]. Luminescence was recorded using Tristar 3 Multimode Reader (Berthold Technologies GmbH & Co.KG, Germany). ATP concentrations were determined using a standard curve generated with known ATP standards provided in the kit and expressed in pmols per 10^{6} CFU [31].

2.6. Chemicals and data analysis

Glucose, peptone, agar, yeast extract, Tris (Carl Roth GmbH, Germany), and other chemical compounds of analytical grade (>98%) were used in this study.

Each data point represents the mean value of at least three independently grown cultures, with a standard deviation of less than 3%. Statistical analysis was performed using GraphPad Prism 8.0.2 software (GraphPad Software, Inc., San Diego, California, USA) with a 2-way ANOVA Tukey test [32]. The graphical working model was prepared using BioRender (BioRender.com; 2026).

3. Results

3.1. The influence of AA on growth and extracellular physicochemical parameters depending on the oxygen availability and S. cerevisiae strain

The results first investigate the concentration-dependent influence of AA on specific growth rate of two *S. cerevisiae* strains (ATCC 9804 and ATCC 13007, respectively) during cultivation under aerobic and oxygen-limited conditions. AA shows strain-; concentration- and oxygen-dependent inhibition of yeast growth (Fig. 1).

10 mM AA inhibits the growth of *S. cerevisiae* ATCC 13007 strain by 1.2-fold under aerobic conditions while the growth rate of ATCC 9804 remains unchanged. 20 mM AA inhibits the growth of *S. cerevisiae* ATCC 9804 and 13007 strains by 1.2-fold under both aerobic and oxygen-limited conditions. High concentration of AA resulted in dramatic inhibition of both strains growth rates. At 50 mM, AA is highly toxic to both strains, with a stronger impact on specific growth rate under oxygen-limited than aerobic conditions. Thus, 50 mM AA exposure results inhibition of *S. cerevisiae* ATCC 9804 strains by 2.8- and 3.8-fold during cultivation under aerobic and oxygen-limited conditions, respectively. In contrast, the growth rate of *S. cerevisiae* ATCC 13007 strain is inhibited by 6.0- and 27.0-fold under the same conditions.

AA exposure effect on extracellular pH and ORP dynamics were monitored during *S. cerevisiae* ATCC 9804 and ATCC 13007 growth under aerobic and oxygen-limited conditions. At the start of cultivation,

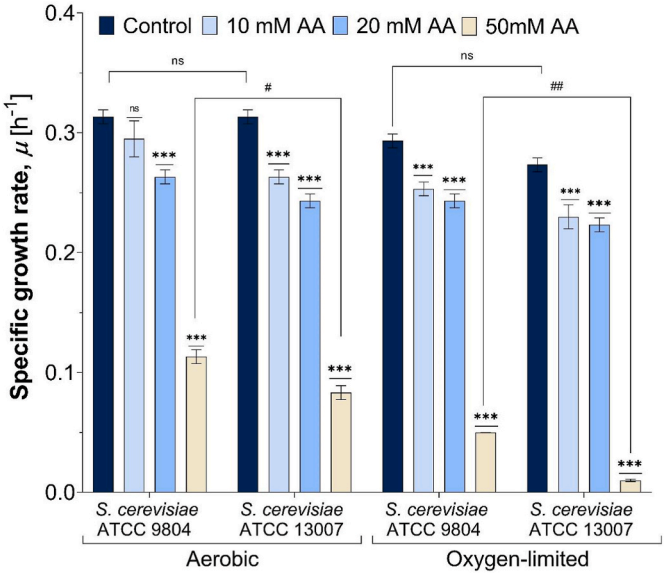


Fig. 1. The impact of 10-50 mM acetic acid (AA) on the specific growth rate of *S. cerevisiae* ATCC 9804 and ATCC 13007 during cultivation under aerobic or oxygen-limited conditions at pH 3.0. Statistical comparisons have been made relative to the control (marked with asterix) or between two strains (marked with pound sign); Statistical significance shown as N = 3; $^{\#}p < 0.05$; $^{\#\#}p < 0.01$, $^{***}p < 0.001$, ns – not significant.

the medium exhibited a pH of ~3.0 and an ORP of ~140 mV (Fig. 2). As growth progressed, a gradual decrease in ORP was observed, coinciding with the exponential growth phase. The highest drop in ORP (~95-115 mV) occurred at the 72 h of growth under aerobic growth (Fig. 2A and B) and at the 24 h of growth under oxygen-limited (Fig. 2C and D) conditions, after which ORP was increased, which correlates with the decrease in OD (data not shown). 10 mM AA has no influence on ORP dynamics of *S. cerevisiae* ATCC 9804 in both aerobic and oxygen-limited conditions, while the maximal ORP drop (~80 mV) decreased during 10 mM AA-exposed *S. cerevisiae* ATCC 13007 growth under aerobic and oxygen-limited conditions. Thus, 10 mM AA exposure effect on ORP dynamics is not oxygen dependent. Redox potential is closely linked to the metabolic pathways of microorganisms, particularly under anaerobic fermentation conditions. It plays an important role in substrate utilization and in directing the formation of specific metabolites. 20-50 mM AA not only reduces the ORP but resulted time-dependent changes in ORP decrease dynamics compared to control, especially, under oxygen-limited conditions (Fig. 2C and D). In parallel, extracellular pH decrease monitored only at the early stages of aerobic growth, with maximum pH drop (~0.6 in *S. cerevisiae* ATCC 9804 culture and ~0.3 in *S. cerevisiae* ATCC 13007 culture) detected at 6th hour, following rapid recovery started from 24th hour (Fig. 2A and B). In contrast, no substantial decrease in extracellular pH were monitored under oxygen-limited condition independent on strain and AA concentration.

Consistent with these observations, the results (Fig. 3) indicate a time-dependent change in medium osmolality strongly influenced by both the strain used and oxygen availability during growth. Moreover, AA alters the dynamics of medium osmolality changes. Interestingly, 10-20 mM AA stress conditions facilitate up to 1.2-fold higher osmolality at 24 h of aerobic growth compared to control conditions. Consequently, the medium osmolality increased up to 96th h of growth with maximum osmolality (626.0 ± 10.0 mOsm kg^{-1}) detected during aerobic growth of *S. cerevisiae* ATCC 9804 (Fig. 3A) under control condition. 10 mM AA exposure at the same conditions resulted in 1.2-fold reduction of medium osmolality, while 20 - 50 mM AA reduces medium osmolality by ~1.5-fold. *S. cerevisiae* ATCC 13007 showed similar medium osmolality changes dynamics (Fig. 3B).

Medium osmolality increased to a maximum of 606 ± 20 mOsm kg^{-1} (ATCC 13007) and 579.0 ± 8.0 mOsm kg^{-1} (ATCC 9804) at 72-96 h during oxygen-limited growth (Fig. 3B–D) similarly to aerobic conditions, followed by a decrease thereafter. 20-50 mM AA stress conditions resulted in time-dependent changes in osmolality. Thus, the maximal osmolality drops (~95 mOsm kg^{-1} for ATCC 9804 and 64-145 mOsm

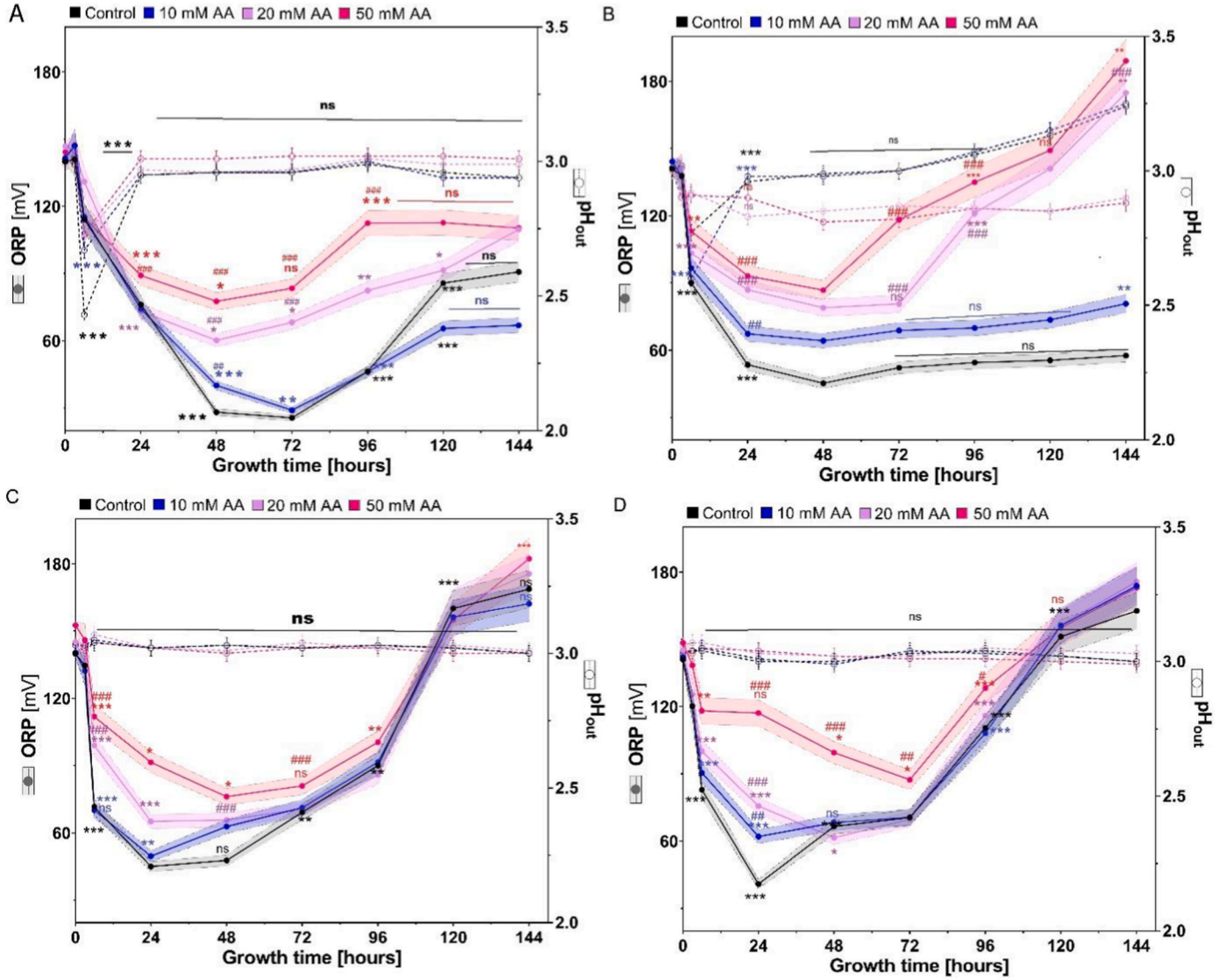


Fig. 2. Monitoring oxidation-reduction potential (ORP) and extracellular pH (pH_{out}) changes dynamics during the growth of *S. cerevisiae* ATCC 9804 (A; C) and ATCC 13007 (B; D) strains exposed to 10-50 mM AA cultivated under aerobic (A; B) or oxygen-limited conditions (C; D) at pH 3.0. N = 3.

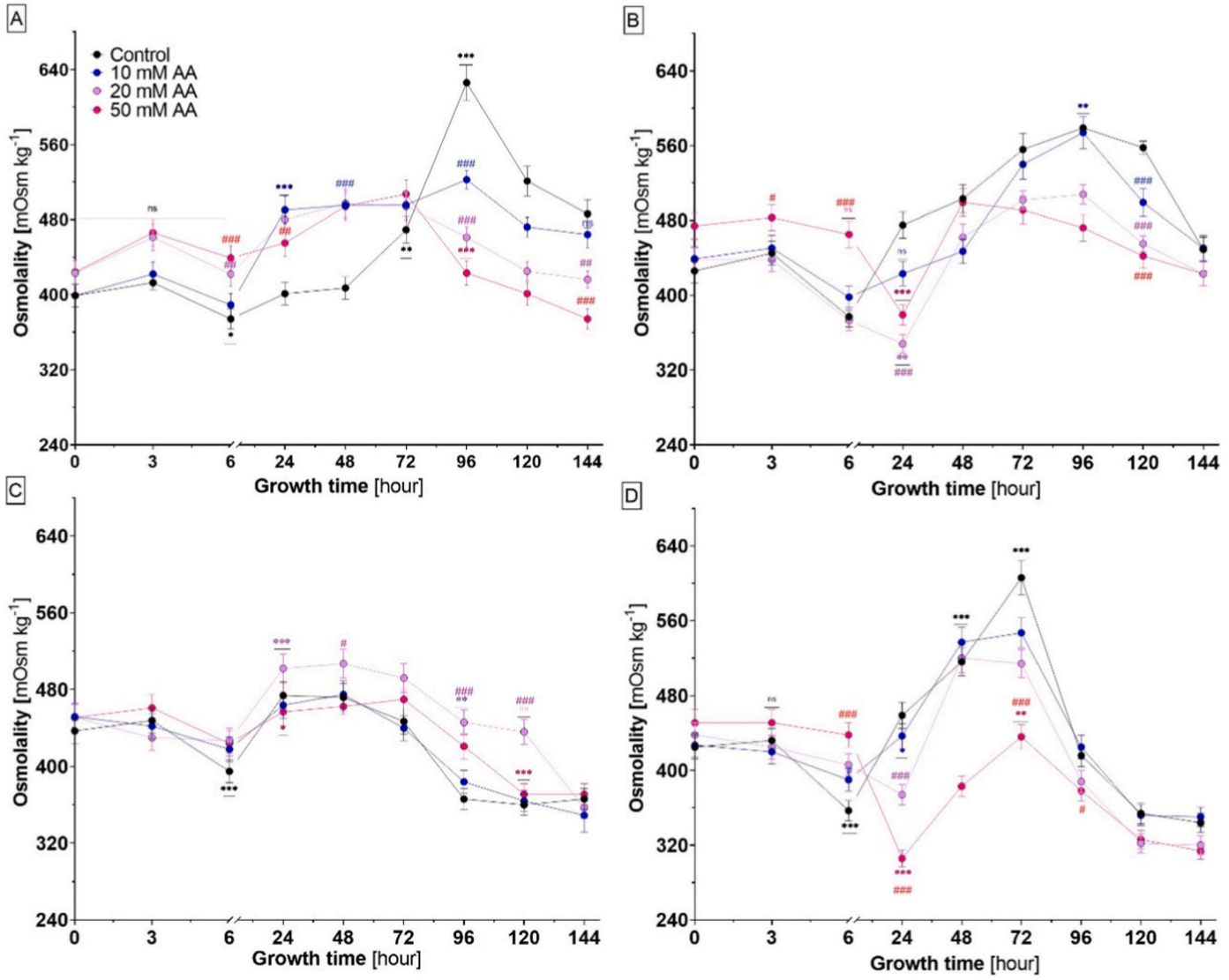


Fig. 3. Extracellular osmolality changes during growth of *S. cerevisiae* ATCC 9804 (A; B) and ATCC 13007 (C; D) cultivated under aerobic (A; C) or oxygen-limited (B; D) conditions upon exposure to 10-50 mM AA at pH 3.0. N = 3; Statistical significance (*p < 0.05; **p < 0.01; ***p < 0.001, ns – not significant) is marked with asterix and denotes comparisons between the indicated time point and the immediately preceding time point within the same condition. Statistical significance ($^{\#}$p < 0.05; $^{\#\#}$p < 0.01; $^{\#\#\#}$p < 0.001) between different conditions is marked with pound sign and denotes comparisons between the value of AA-treated group to the control group from inditical time points.

kg^{-1} for ATCC 13007) were detected at 24th h of oxygen-limited growth upon exposure to 20-50 mM AA, while in control and 10 mM AA-exposed culture, the minimal osmolality detected at 6th h of growth.

3.2. Ion flux rate changes under AA stress depending on growth conditions

Ion fluxes were determined across the intact plasma membrane of *S. cerevisiae* ATCC 9804 and 13007 cells cultivated under aerobic or oxygen-limited conditions in control or upon AA-treated conditions. Results show that total J_H^+ was ~7.0 and ~14.0-fold higher in *S. cerevisiae* ATCC 9804 and ATCC 13007 strains, respectively, cultivated under oxygen-limited conditions compared to aerobic growth under control conditions (Fig. 4). Despite total J_{Na}^+ remaining constant independently of oxygen availability, under the same conditions DCCD-sensitive J_{Na}^+ was 7.0-13.0-fold higher than the same value obtained under aerobic conditions. Meanwhile, total and DCCD-sensitive J_K^+ exhibited no significant variations depending on oxygen availability.

10-50 mM AA induces concentration-dependent stimulation of J_H^+ systems in both *S. cerevisiae* ATCC 9804 and ATCC 13007 strains during aerobic growth but not under oxygen-limited growth (Fig. 4). Thus, 10 mM AA stimulates total J_H^+ in *S. cerevisiae* ATCC 9804 and ATCC 13007 by respectively 5.0- and 4.0-fold (Fig. 4A; C), while 20-50 mM AA exposure results in 9.0-10.0-fold increase in total J_H^+ for the same conditions. In addition to increasing total J_H^+, AA exposure also enhances the contribution of DCCD-sensitive J_H^+. At 10 mM AA, DCCD-sensitive J_H^+ increased by ~30% in *S. cerevisiae* ATCC 9804, whereas the same concentration resulted in a ~200% increase in *S. cerevisiae* ATCC 13007. Meanwhile. total J_H^+ remains relatively stable during AA exposure under oxygen-limited conditions (Fig. 4B–D): 10 and 20 mM AA exposure results no significant change in total J_H^+ of *S. cerevisiae* ATCC 9804, and only 50 mM AA treatment increased total J_H^+ by ~20%, however, the DCCD-sensitive J_H^+ increased during AA exposure in *S. cerevisiae* ATCC 9804 cultivated under oxygen-limited conditions, showing an approximately linear increase across the tested AA concentrations (Fig. 4B). In contrast, total and DCCD-sensitive J_H^+ increased by ~40% and 60%, respectively, in *S. cerevisiae* ATCC 13007 under 10 mM AA stress conditions and further increase of AA concentration decrease total and

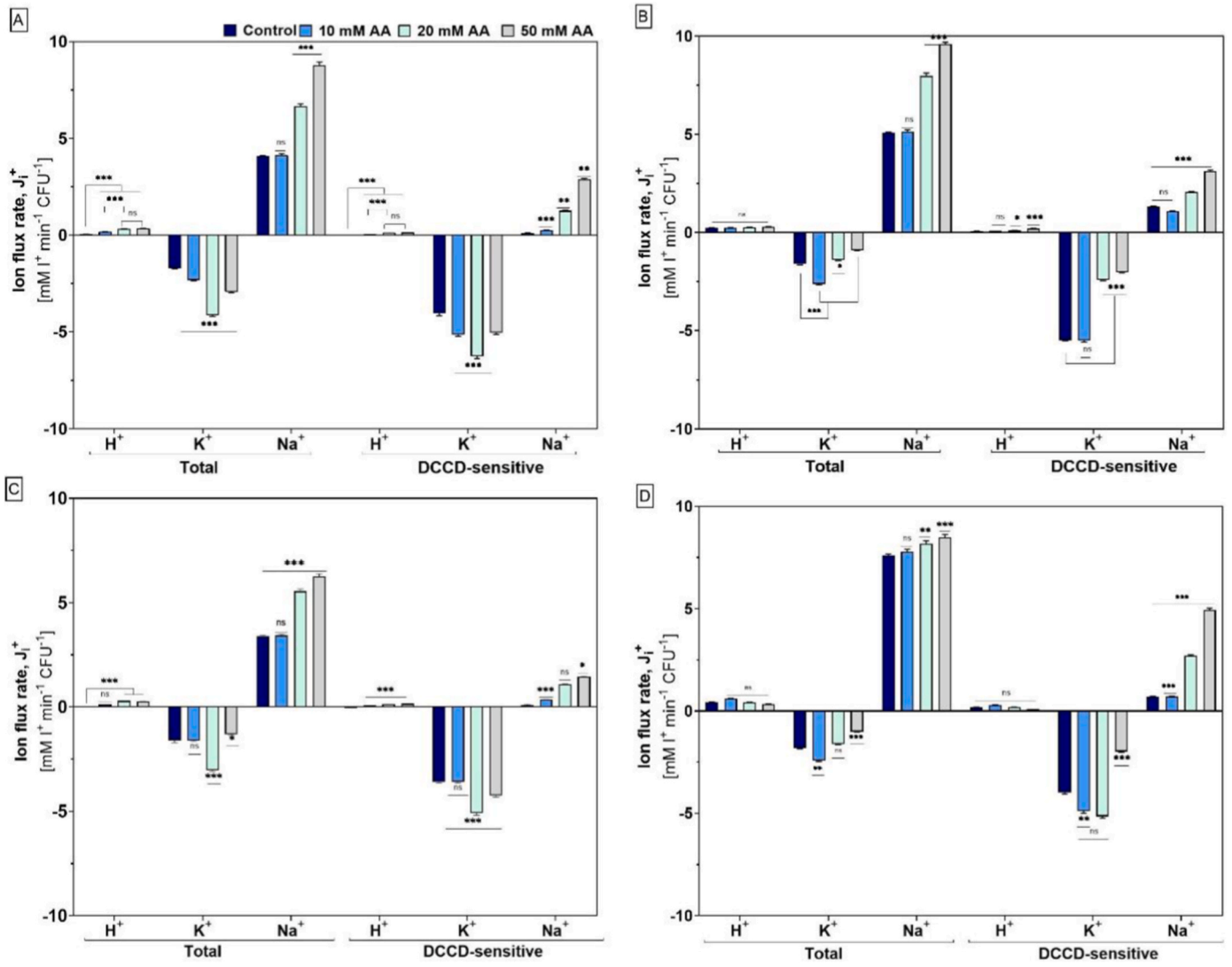


Fig. 4. Total and DCCD-sensitive ion flux (J_i^+) dynamics in intact *S. cerevisiae* ATCC 9804 (A; B) and ATCC 13007 (C; D) cells cultivated under aerobic (A; C) or oxygen-limited (B; D) conditions during exposure to 10-50 mM AA at pH 3.0. egative values indicate net ion uptake and positive values indicate net ion efflux. DCCD-sensitive flux represents the difference between total flux and the flux measured after DCCD treatment. Data are means ± SD of three independent cultures. Statistical significance: N = 3, *p < 0.05; **p < 0.01; ***p < 0.001, ns - not significant.

DCCD-sensitive J_H^+ (Fig. 4D), which correlates with decrease in specific growth rate (Fig. 1).

Exposure to 10 mM AA results in non-significant changes in total J_{Na}^+, regardless of strain or oxygen availability. However, the DCCD-sensitive J_{Na}^+ increases 2.5-fold in *S. cerevisiae* ATCC 9804 and 3.5-fold in *S. cerevisiae* ATCC 13007, while under oxygen-limited conditions, the DCCD-sensitive J_{Na}^+ shows no significant changes in either strain. Total J_{Na}^+ increases by 60-110% under 20-50 mM AA stress conditions in *S. cerevisiae* ATCC 9804 and ATCC 13007 strains. Remarkably, DCCD-sensitive J_{Na}^+ increases during AA exposure in *S. cerevisiae* ATCC 9804 cultivated under aerobic conditions, showing an approximately directly proportional dependence on AA concentration (Fig. 4A). DCCD-sensitive J_{Na}^+ increased across the tested AA concentrations, with a nonlinear pattern in ATCC 13007 (Fig. 4C). In contrast, total J_{Na}^+ has no significant changes upon 10-50 mM AA exposure of *S. cerevisiae* ATCC 13007 cells cultivated under oxygen-limited conditions (Fig. 4D). However, DCCD-sensitive J_{Na}^+ increase by 3.8- and 7.0-fold during growth of the same strain under respectively 20 mM and 50 mM AA stress conditions at pH 3.0. 20 and 50 mM AA exposure results up to 1.5-2.5-fold increase of total and DCCD-sensitive J_{Na}^+ (Fig. 4C).

Likewise, 10 mM AA exposure results 40% and 60% increase in total J_K^+ of *S. cerevisiae* ATCC 9804 cultivated under respectively aerobic and oxygen-limited conditions (Fig. 4A; B). On the other hand, DCCD-sensitive J_K^+ increases by ~30% during 10 mM AA exposure under aerobic conditions. 20-50 mM AA exposure results in 2.5- and 1.8-fold increase of total J_K^+ in *S. cerevisiae* ATCC 9804 cultivated under aerobic conditions, while DCCD-sensitive J_K^+ increased by ~60% during 20 mM and by ~30% during 50 mM AA exposure under the same conditions (Fig. 4A). 10 mM AA exposure results in non-significant changes of total and DCCD-sensitive J_K^+ in *S. cerevisiae* ATCC 13007 under both aerobic and oxygen-limited conditions (Fig. 4C; D). Exposure of *S. cerevisiae* ATCC 13007 cells to 20 mM AA has district phenotypes depending on oxygen availability during growth: under aerobic conditions total and DCCD-sensitive J_K^+ increases by respectively 70% and 40%, while under oxygen-limited conditions total J_K^+ remains unchanged and DCCD-sensitive J_K^+ increases by only by ~30%. 50 mM AA seriously impairs potassium transport systems in either strain, resulting in relative decline of total and DCCD-sensitive J_K^+. The same tendency was shown under oxygen-limited growth of *S. cerevisiae* ATCC 9804 with inhibition observed starting from 20 mM.

Under aerobic conditions, AA progressively increased the DCCD-sensitive Na^+/H^+ ratio, whereas the magnitude of the K^+/H^+ ratio

decreased with increasing AA concentration (Fig. 5A and B). These changes indicate a shift from K^+ uptake relative to H^+ efflux toward greater Na^+/H^+ exchange under increasing AA stress. Under oxygen-limited conditions, ATCC 9804 displayed a markedly higher basal Na^+/H^+ ratio than under aerobic growth, whereas the ratio in ATCC 13007 was comparatively lower (Fig. 5A and B). At 10 mM AA, the Na^+/H^+ ratio remained relatively stable in both strains, but increased at 20 mM AA. At 50 mM AA, the ratio decreased in ATCC 9804 but continued to increase in ATCC 13007, indicating strain-specific responses to severe AA stress. In contrast, the DCCD-sensitive K^+/H^+ ratio was substantially lower under oxygen limitation and declined further in ATCC 9804 at higher AA concentrations, while remaining relatively stable in ATCC 13007.

To place the observed ion-flux responses in the context of established molecular mechanisms of AA tolerance, the reported regulation and functional roles of major yeast ion transporters and AA-responsive regulators were compiled from the literature (Table 2). These include Pma1/2, Vma1, Nha1/Nhx1, Trk1/2 and Tok1, as well as AA-responsive regulatory and acetate transport systems. The literature summarized in Table 2 indicates that the regulation of ion-homeostasis systems during AA stress is strongly dependent on growth and oxygen conditions. Thus, the observed changes in ion fluxes likely reflect coordinated remodeling of multiple transport processes rather than activation of a single transporter. This interpretation is consistent with our previous observation that respiratory metabolism can enhance AA tolerance [33].

3.3. Intracellular pH, transmembrane pH gradient and intracellular ATP level changes under AA stress depending on growth conditions

Intracellular pH (pH_{in}) and transmembrane pH gradient (ΔpH) were determined in mid-exponential growing *S. cerevisiae* ATCC 9804 and ATCC 13007 exposed to increasing AA concentrations (10-50 mM) cultivated under aerobic and oxygen-limited conditions. Results indicate that both strains exhibited intracellular pH values between 6.20 and 6.30 and positive transmembrane pH gradients of 3.20–3.30, which were comparable under both growth conditions (Fig. 6).

S. cerevisiae ATCC 9804 maintained an intracellular pH of 6.30 ± 0.10 in control and in the presence of 10 mM AA under aerobic conditions (Fig. 6A). At higher AA concentrations, intracellular pH decreased to 6.00 ± 0.05 at 20 mM AA and to 5.9 ± 0.03 at 50 mM AA. The corresponding transmembrane pH gradients (Fig. 6C) declined from 3.3 ± 0.02 in control to 3.0 ± 0.02, 2.7 ± 0.02, and 2.6 ± 0.02 at 10, 20, and 50 mM AA, respectively. *S. cerevisiae* ATCC 13007 showed a similar trend; however, a decrease in intracellular pH of approximately 0.4 units was already observed at 10 mM AA, whereas no significant change was detected in ATCC 9804 at this concentration. The largest decrease in

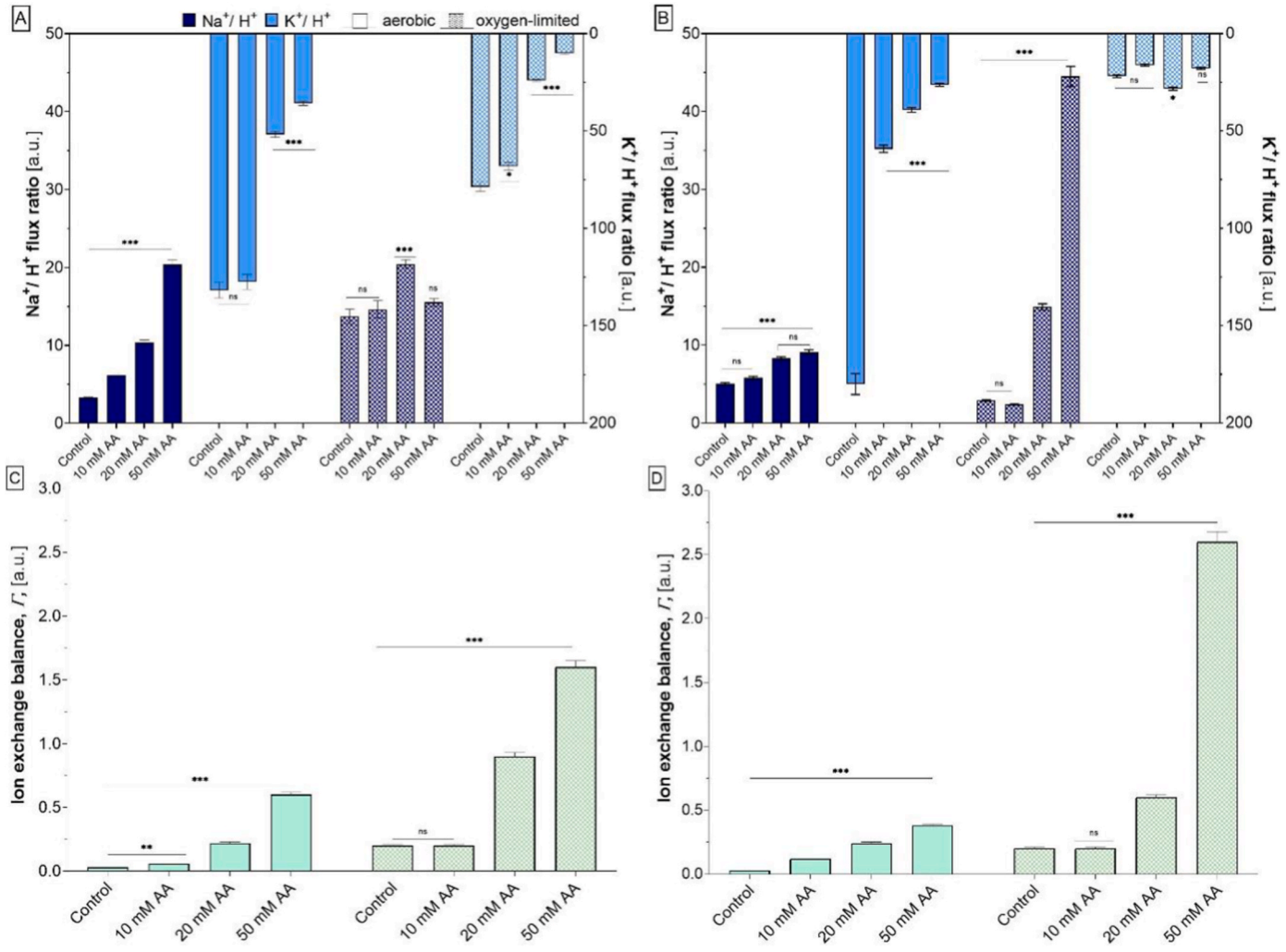


Fig. 5. DCCD-sensitive Na^+/H^+ and K^+/H^+ ratios (A; B) and ion exchange balance, *Γ* (C; D) in *S. cerevisiae* ATCC 9804 (A; C) and ATCC 13007 (B; D) cells cultivated under aerobic or oxygen-limited conditions upon exposure to 10-50 mM AA. The DCCD-sensitive Na^+/H^+ and K^+/H^+ exchange ratios were calculated from the corresponding DCCD-sensitive fluxes. The ion exchange balance (Γ) was calculated as the ratio of the combined DCCD-sensitive Na^+ and H^+ effluxes to the absolute value DCCD-sensitive K^+ influx (For more see Materials and methods). N = 3, Statistical significance, *p < 0.05; **p < 0.01; ***p < 0.001, ns - not significant.

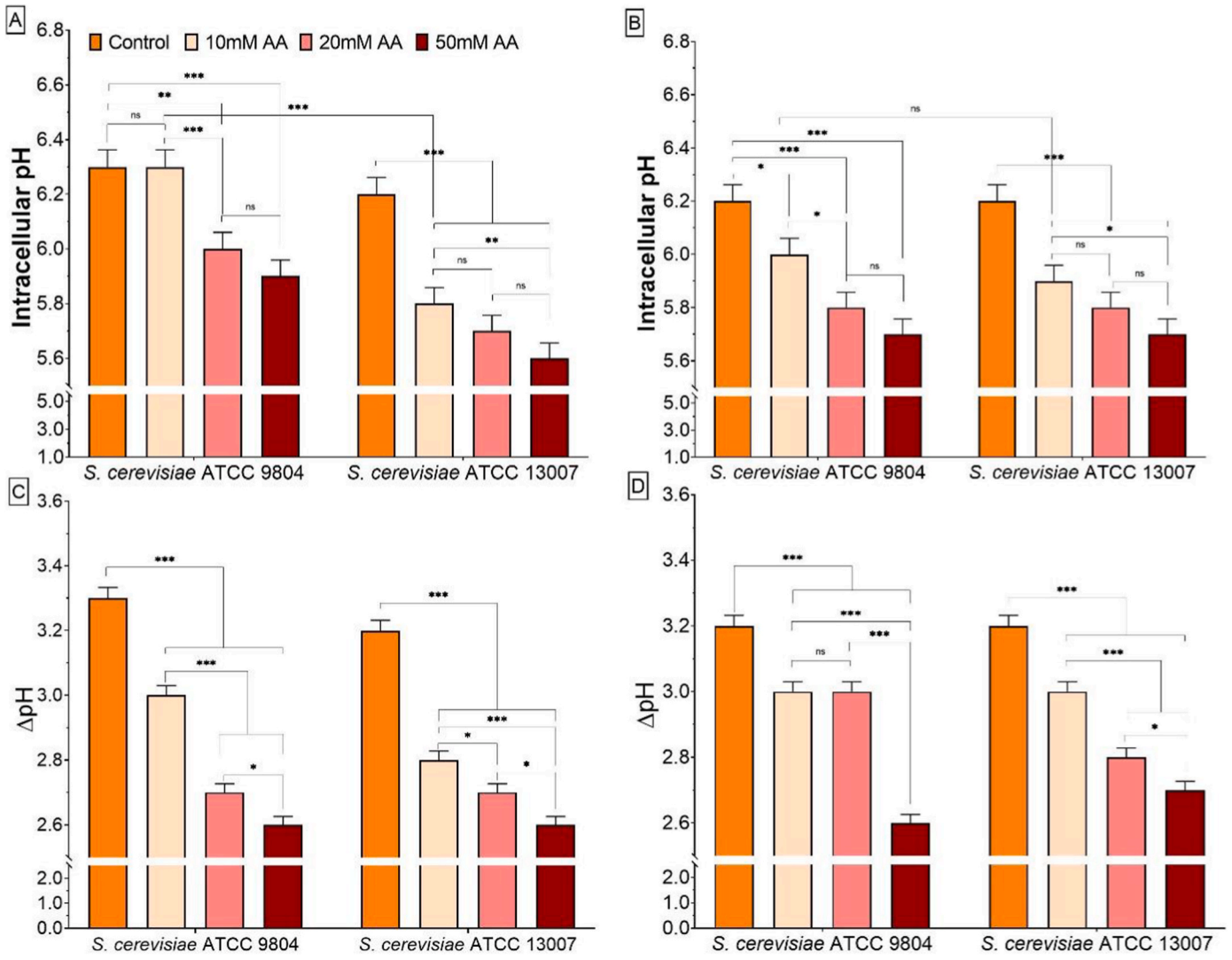


Fig. 6. Intracellular pH, pH_{in} (A; B) and ΔpH (C; D) changes of *S. cerevisiae* ATCC 9804 and ATCC 13007 strains during exposure to 10-50 mM AA under aerobic (A; C) or oxygen-limited (B; D) conditions. ΔpH was calculated as pHin − pHout. Data are means ± SD of three independent cultures (n = 3). Statistical significance: N = 3; *p < 0.05; **p < 0.01; ***p < 0.001, ns – not significant.

intracellular pH (~0.6) was observed in ATCC 13007 under 50 mM AA during aerobic growth (Fig. 6A). In parallel, ΔpH decreased from 3.20 ± 0.03 in control cultures to 2.80 ± 0.02, 2.70 ± 0.02, and 2.60 ± 0.02 at 10, 20, and 50 mM AA, respectively.

Intracellular pH and transmembrane proton gradient (ΔpH) decreased progressively with increasing AA concentration in both strains under oxygen-limited conditions as well (Fig. 6B; D). In *S. cerevisiae* ATCC 9804, pH_{in} declined from 6.20 ± 0.06 in control culture to 6.00 ± 0.05 at 10 mM AA, 5.80 ± 0.05 at 20 mM AA, and 5.70 ± 0.05 at 50 mM AA. The corresponding ΔpH (3.20 ± 0.03 in control) decreased by ~0.6 at 50 mM AA. Similar decreases in intracellular pH and ΔpH were observed in ATCC 13007 grown under oxygen-limited conditions. Overall, increasing AA concentrations were associated with a progressive reduction in intracellular pH and ΔpH in both *S. cerevisiae* strains under both aerobic and oxygen-limited conditions, with intracellular pH values consistently higher in ATCC 9804 than in ATCC 13007 across most conditions.

Next, our study focuses on intracellular proton concentration ($[H^+]_{in}$) calculated from measured pH_{in} values in *S. cerevisiae* ATCC 9804 and ATCC 13007 under aerobic or oxygen-limited conditions (Table 1). Results indicate that under control conditions, independent of oxygen availability, intracellular protons concentration in both strains cytoplasm ranged from 0.5 to 0.6 μM and AA treatment results up to 4.0-fold increase in intracellular proton concentration reaching up to

Table 1
Intracellular proton concentrations (μM) during AA stress in *S. cerevisiae* cells grown at pH 3.0 under aerobic or oxygen-limited conditions. N = 3.

	***S. cerevisiae* ATCC 9804**			
	Control	**10 mM AA**	**20 mM AA**	**50 mM AA**
aerobic growth	0.50 ± 0.01	0.50 ± 0.01^{ns}	1.00 ± 0.05***	1.26 ± 0.03***
oxygen limited growth	0.63 ± 0.03$^{\#\#}$	1.00 ± 0.05***	1.58 ± 0.06***	2.00 ± 0.05***
	***S. cerevisiae* ATCC 13007**			
	Control	**10 mM AA**	**20 mM AA**	**50 mM AA**
aerobic growth	0.63 ± 0.03	1.58 ± 0.05***	2.00 ± 0.07***	2.51 ± 0.12***
oxygen limited growth	0.63 ± 0.04^{ns}	1.26 ± 0.07***	2.00 ± 0.10***	2.51 ± 0.14***

Statistical comparisons have been made relative to the control (marked with asterix) or between two control groups grown under aerobic or oxygen-limited conditions (marked with pound sign); Statistical significance shown as $^{\#\#}p < 0.01$; ***p < 0.001, ns – not significant.

Table 2
Reported key transcriptional regulators and transport-related genes involved in acetic acid stress response and adaptation.

	Gene	Expression	Gene product function	Expression conditions tested	Reference
Transcriptional factors	*haa1*	Expressed/Active	master transcription factor of AA response genes	toxic levels of AA, early adaptation phase; pH 3.5-4.5; aerobic batch culture	[34]
	hrk1	Expressed/Active	plasma membrane H^+-ATPase (Pma1) and ion exchangers, e.g. Nha1 activation, intracellular pH and membrane potential control	sub-lethal or lethal toxic acetic acid levels, pH 3.5-4.5, aerobic batch culture	[9]
	hog1	Expressed/Transiently Phosphorylated (Activated)	osmotic and general stress response/triggers endocytosis and degradation of the *FPS1* aquaglyceroporin channel to restrict passive influx of undissociated AA	acute or high, toxic concentrations of acetic acid or acetate, pH 4.0-4.5; aerobic to oxygen-limited batch culture	[35–37]
	pdr1	Expressed	upregulates ATP-binding cassette efflux pumps to remove lipophilic stressors and toxic anions.	industrial fermentation or minimal media supplemented with severe organic acid, ethanol, or xenobiotic shocks, pH 3.5 – 4.5; aerobic, anaerobic, or oxygen-limited; batch and continuous cultures	[34]
Acetate detoxification and export genes	*tpo2/3*	upregulated	acetate efflux	Mineral media containing severe concentrations of acetic acid (e.g., 50 mM acetate). pH 4.0; aerobic batch culture.	[5]
	aqr1	downregulated	Acetate transporter, multidrug resistance		
	ady2	downregulated by glucose; expressed/upregulated under non-fermentable carbon source or post-adaptation	Acetate/monocarboxylate transporter; active uptake of acetate anion	ethanol, glycerol, or post-adaptation media with weak organic acids; pH 4.0 – 5.5; Aerobic to microaerophilic; batch and continuous culture.	[38]
	jen1	Downregulated by glucose; Upregulated during glucose exhaustion/monocarboxylate growth	Monocarboxylate transporter (lactate, pyruvate, acetate, micronutrients proton symporter)	non-fermentable carbon media or when glucose drops near zero during late-stage processing; pH 4.0 – 5.0; aerobic batch culture	[9,39]
Ion homeostasis and pH_{in} regulation	*pma1/2*	upregulated/essential	plasma membrane H^+-ATPase; major proton pump	Synthetic or industrial fermentation broth during exposure to weak organic acid stress; pH 3.0 – 4.5; Aerobic to oxygen-limited; Batch and continuous culture	[5,9]
	vma1	Expressed/Essential	catalytic subunit (A) of the V-type H^+-ATPase; pumps cytosolic protons into the vacuole to safeguard intracellular neutral pH	organic acid-stressed fermentation media; pH 3.0 – 4.5; aerobic to anaerobic; batch and continuous culture	[40,41]
	trk1/2	Expressed	high-affinity potassium transporters; work with *HRK1* to drive active K^+ accumulation, offsetting the proton-induced depolarizing drop in membrane potential.	Potassium-depleted media or during active proton stress caused by weak organic acids; pH 3.5 – 4.5; aerobic batch culture	[9]
	tok1	Expressed	outward-rectifying potassium channel; acts as an electrical safety valve, releasing intracellular K^+ to balance sudden membrane depolarizations or severe acid shocks	chemically induced stress, high external potassium, or deep weak organic acid adaptation; pH 4.0 – 6.0; aerobic to oxygen-limited batch culture	[42]
	nha1	Expressed/Co-regulated by HRK1	plasma membrane Na^+,K^+/H^+ antiporter; exports excessive alkali cations to preserve cell volume and control plasma membrane electrochemical potential under low pH.	Synthetic media under potassium/sodium limitation or weak acid stress; pH 3.5 – 4.0; aerobic; batch and continuous culture	[9]
	nhx1	Expressed/Dominant in intracellular pH control	endosomal/vacuolar Na^+, K^+/H^+ exchanger; counteracts V-ATPase' proton accumulation inside compartments to adjust vesicular pH and salt tolerance	Salt-stressed or weak organic acid-stressed minimal/rich media; pH: pH 3.0 – 4.5; aerobic or anaerobic; batch culture	[9,43]

~2.5 μM in 50 mM AA exposed *S. cerevisiae* ATCC 13007 cells. 10 mM AA treatment under aerobic conditions results in no significant changes of intracellular proton concentration of *S. cerevisiae* ATCC 9804 cells which correlate with no significant changes in specific growth rate under the same conditions (Fig. 1). Instead, 10 mM AA increases protons intracellular concentration by ~1.0 μM in *S. cerevisiae* ATCC 13007 under same conditions. 20-50 AA treatment increases $[H^+]_{in}$ by 0.5-0.8 μM in ATCC 9804 and by 1.4-1.9 μM in ATCC 13007 under aerobic conditions. Even though small changes in intracellular pH, $[H^+]_{in}$ study shows significant differences in intracellular acidification depending on oxygen availability. Thus, under oxygen-limited conditions, 10 mM AA already results in 1.6- and 2.0-fold increase of $[H^+]_{in}$ in *S. cerevisiae* ATCC 9804 and ATCC 13007 strains, respectively. Furthermore, 20-50 mM AA results in ~3.0- and ~4.0-fold increase of $[H^+]_{in}$ for the same strains, respectively.

Intracellular ATP levels were strongly dependent on AA concentration, oxygen availability, and strain (Fig. 7). *S. cerevisiae* ATCC 9804 exhibited a progressive increase in intracellular ATP at 10 and 20 mM AA under aerobic conditions (Fig. 7A). Thus, ATP levels increased by approximately ~25% at 10 mM and ~50% at 20 mM AA relative to control (~833 pmol per 10^6 CFU). At 50 mM AA, ATP level decreased to ~926 pmol per 10^6 CFU. In ATCC 13007, the control culture showed a higher basal ATP level (~1355 pmol per 10^6 CFU). ATP level increased to ~1521 pmol per 10^6 CFU at 10 mM AA, whereas 20 and 50 mM AA resulted in lower ATP levels, with up to 30% decrease in intracellular ATP level at 50 mM AA exposure relative to control.

Under oxygen-limited conditions, both strains showed higher basal intracellular ATP level compared to aerobic conditions (Fig. 7B). ATP level increased by ~50% and ~65% in ATCC 9804 at 10 and 20 mM AA stress conditions, respectively. At 50 mM AA, ATP level changes were like those observed under aerobic conditions, with pronounced decline compared to 20 mM AA stress condition. ATP level increased by only ~20% in ATCC 13007 cells during oxygen-limited growth under 20 mM AA exposure, while 50 mM AA caused a dramatic ATP depletion, with intracellular ATP falling to ~276 pmol per 10^6 CFU or ~80% below the control level (Fig. 7B).

Overall, moderate AA concentrations, particularly 20 mM, stimulated intracellular ATP accumulation in both strains, which correlates

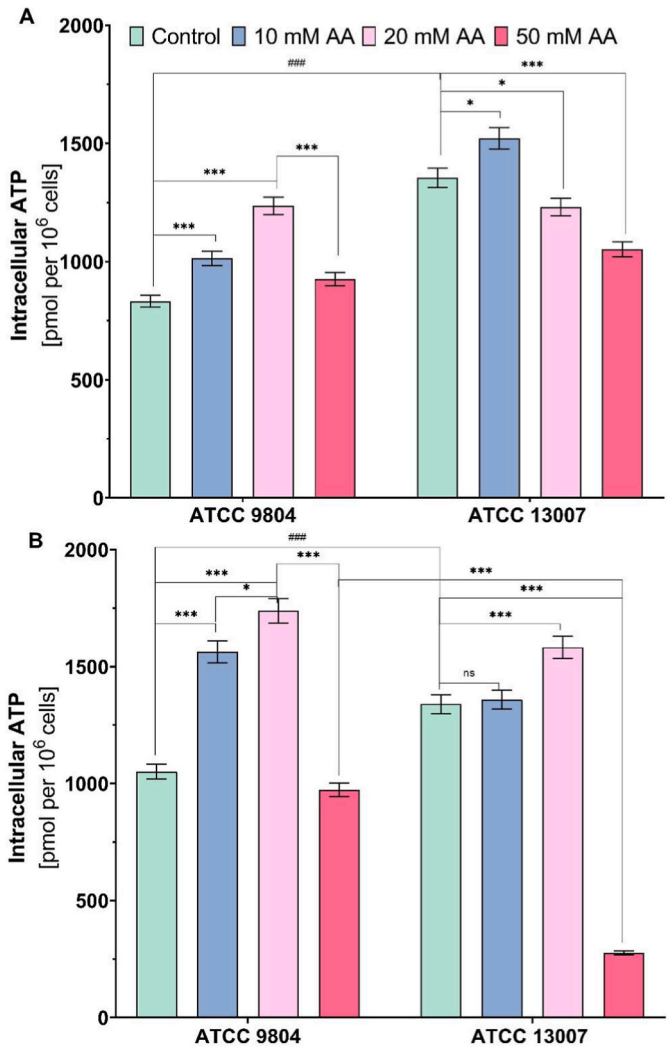


Fig. 7. Changes in intracellular ATP levels in *S. cerevisiae* ATCC 9804 and ATCC 13007 strains exposed to AA stress during aerobic (A) or oxygen-limited (B) growth. Statistical comparisons have been made relative to the control (marked with asterix) or between two strains (marked with pound sign); Statistical significance shown as $^{###}p < 0.001$; *p < 0.05; **p < 0.01; ***p < 0.001, ns – not significant, N = 3.

with increased DCCD-sensitive proton flux. The strongest response observed in ATCC 9804 under oxygen-limited conditions, while under same conditions, ATCC 13007 showed only minimal increase in ATP level. In contrast, severe AA stress at 50 mM resulted in substantial ATP depletion, most prominently in ATCC 13007 under oxygen limitation.

4. Discussion

Weak organic acids, such as AA, impose multifactorial stress on *S. cerevisiae*, affecting growth, intracellular pH homeostasis, redox balance, and ion transport. While AA toxicity has been extensively studied [9,33,44], comparatively limited data are available concerning how oxygen levels modulate these responses at the level of ion fluxes and intracellular proton handling. We investigated the effects of AA on the ion fluxes across plasma membrane and intracellular acidification patterns in *S. cerevisiae* to elucidate strain-specific and oxygen-dependent mechanisms of AA tolerance.

Our results demonstrate that AA toxicity strongly depends on both strains background, AA concentration and oxygen availability. *S. cerevisiae* ATCC 9804 exhibited higher tolerance to AA than ATCC 13007, especially under aerobic conditions (Fig. 1). The combined ion-flux and ATP data indicate that oxygen availability does not simply alter the individual transport processes but changes their coordination. Under aerobic conditions, AA stress was accompanied by a strong increase in DCCD-sensitive proton efflux, consistent with increased ATP-dependent proton extrusion. Under oxygen limitation, basal proton flux was already elevated, while increasing AA concentration produced a smaller increase in total proton flux and a progressive redistribution between DCCD-sensitive and DCCD-insensitive components. At the same time, K^+/H^+ coupling declined and the ion exchange balance increased, indicating that proton efflux was no longer efficiently coordinated with K^+ uptake. Thus, oxygen limitations appear to reduce the capacity to maintain coordinated ion transport as AA stress increases, rather than simply suppressing individual transporters.

Oxygen limitation markedly stimulates AA toxicity in both strains, particularly at high AA concentrations. Despite aerobic fermentation in Crabtree-positive yeast, oxygen availability substantially mitigated AA toxicity due to facilitating of the heme, sterols and unsaturated fatty acids synthesis, promoting cell growth and improving fermentative capacity [45]. The results obtained consistent with our previous data [33] showing that yeast viability increases from fermentation-to respiration-type metabolism, and that ATCC 9804 is more viable under AA stress compared to ATCC 13007 strain.

Changes in ORP (Fig. 2) closely followed growth dynamics and were strongly influenced by AA concentration and strain. The attenuated ORP decrease observed in ATCC 13007 under AA stress suggests impaired metabolic activity and redox balancing, consistent with its higher growth sensitivity. Despite the low initial extracellular pH (~3.0) and observed changes in specific growth rate and viability of strains, the results showed that extracellular pH mainly remains stable with maximum pH_{ex} drop observed at 6-24th hour of growth (Fig. 2). The transient extracellular acidification observed during early aerobic growth likely reflects organic acid production and proton release associated with metabolic activity [46]. This may be attributed to the intracellular accumulation of organic acids which balances the extracellular acidity and hence helps maintain the transmembrane proton gradient. Here, we show that AA-induced disruption of pH and redox homeostasis [47] is strongly modulated by oxygen availability and differs markedly between strains at the level of ion fluxes.

Results indicate (Fig. 3) that similarly to extracellular redox potential, AA-induced alterations in medium osmolality reflect changes in metabolite secretion, ion exchange, and possibly cell lysis at high AA concentrations, particularly under oxygen-limited conditions. The initial reduction of medium osmolality may be associated with the depletion of glucose over time. Further increase in medium osmolality can be attributed to glycerol biosynthesis. Earlier, it was shown [48] that AA and acidic pH can induce glycerol synthesis, which affect ethanol yield, while also acting as a stress-buffering agent due to its role as a precursor for fatty acids and plasma membrane components. Indeed, our previous results also highlight that under oxygen-limited conditions, the *S. cerevisiae* ATCC 13007 strain can produce ~2.0-fold more glycerol compared to *S. cerevisiae* ATCC 9804 [13]. Decrease in medium osmolality at late stages can be due to fermentation products consumption due to glucose depletion [3,49]. Changes in extracellular ORP and osmolality dynamics indicate time-resolved shift in metabolism, indicating inhibitory effect of AA on metabolic activity of strains depending on both strain type and oxygen availability. This was consistent with earlier study [40] showing that a reduction in intracellular ATP pools, coupled with disruptions in proton gradients under AA stress, hinders the ATP-dependent symport of nutrients.

Monovalent ions play a crucial role in adaptation to stress conditions via regulation of distinct physiological parameters such as cell volume, plasma membrane potential, and intracellular pH [50,51]. While individual ion transporters involved in AA tolerance have been studied, how oxygen availability modulates the balance of ion fluxes across the plasma membrane remained unexplored. Here, we show that AA-induced pH stress is fundamentally reshaped by oxygen availability,

resulting in strain-specific reorganization of Na^+, K^+, and H^+ fluxes. The study investigates pronounced stimulation of proton efflux systems under AA stress, particularly during aerobic growth (Fig. 4A; C). AA exposure led to strong, concentration-dependent increases in total and DCCD-sensitive J_H^+. Because Pma1 is the major plasma-membrane H^+-ATPase in *S. cerevisiae*, this response is consistent with increased Pma1-dependent proton efflux, although transporter-specific activity was not directly measured in the present study. This interpretation is consistent with previous studies identifying the upregulation of Pma1, as a major plasma-membrane H^+ pump required for intracellular pH control during weak-acid stress, and Vma1, which contributes to intracellular proton import to vacuoles (Table 2). Hrk1 has also been reported to regulate Pma1 and ion-exchange systems during AA stress, providing an additional regulatory component that may contribute to the increased proton extrusion observed here [5,9]. Our data reveal that AA stress triggers a disproportionate increase in DCCD-sensitive J_H^+, particularly under aerobic conditions, indicating a strain-specific energetic burden associated with Pma1 activation [9]. This response was more pronounced in ATCC 13007, indicating a greater reliance on ATP-dependent proton extrusion under AA stress. However, the ATP measurements (Fig. 7) suggest that the higher DCCD-sensitive H^+ flux observed in ATCC 13007 combined with relatively lower ATP levels under stress conditions compared to ATCC 9804 strain, may represent a greater energetic burden rather than a more efficient adaptive response. Furthermore, 7.0-14.0-fold higher total J_H^+ (Fig. 4B; D), observed under oxygen-limited conditions, may reflect partial membrane damage or lipid rearrangement induced by acidic pH and oxygen-limitation, which inhibit cell membrane reconstruction. The pronounced increase in J_H^+ under oxygen limitation suggests compromised membrane organization, consistent with previous studies showing impaired sterol- and sphingolipid-dependent compartmentalization of Pma1 under AA stress [7,9,52]. On the other hand, it was shown that AA stress can decrease the ergosterol content [53] and alter sphingolipid content [54], affecting cell fate, protein trafficking, signaling pathways and membrane permeability.

Although total J_H^+ remained relatively constant despite increasing AA concentrations, under oxygen-limited conditions, the DCCD-sensitive J_H^+ increased. This pattern suggests a redistribution of proton transport mechanisms rather than a net increase in proton efflux capacity. To mitigate the effects of AA stress, yeast cells trigger the ATP-dependent efflux of protons and acetate from the cell [9]. Given that plasma membrane proton pumping is ATP-dependent, this shift is expected to increase cellular energy demand and require enhanced ATP availability to sustain pH and ion homeostasis. Whether cells can meet this increased energetic demand may therefore represent an important determinant of AA tolerance and may contribute to the observed reduction in growth, especially at high AA concentration, as was shown in Fig. 1, which highly correlated with literature data [9]. The inability of ATCC 13007 to further increase J_H^+ under oxygen limitation during 50 mM AA treatment (Fig. 4D) may contribute to the greater intracellular acidification, which correlates with growth inhibition observed under these conditions.

To directly assess whether the altered proton transport observed under AA stress was associated with changes in cellular energy status, intracellular ATP levels were quantified (Fig. 7). The ATP response revealed a concentration-, strain-, and oxygen-dependent pattern. Under aerobic conditions. The increase in ATP under moderate AA stress is consistent with the enhanced DCCD-sensitive H^+ efflux observed in Fig. 4 and supports the interpretation that active proton extrusion imposes an increased energetic demand during AA adaptation. In particular, the pronounced increase in ATP levels in ATCC 9804 can meet the energy requirements associated with proton pump activity and ion homeostasis. Conversely, ATCC 13007 cells maintained lower ATP levels under stress conditions compared to ATCC 9804, which may account for their inefficient proton homeostasis and subsequent failure to resist stress.

ATP depletion suggests failure of this energetic compensation, which may contribute to may contribute to impaired maintenance of ion and pH homeostasis and ultimately to loss of metabolic activity [55,56]. At 50 mM AA, intracellular ATP declined in both strains, with the strongest depletion observed in ATCC 13007 under oxygen-limited conditions. This severe depletion coincided with the strong inhibition of growth (Fig. 1), impaired ion transport (Figs. 4 and 5), and pronounced intracellular acidification (Fig. 6) observed under the same conditions. These results suggest that, beyond a threshold of AA stress, the energetic cost of maintaining proton and ion homeostasis may exceed the capacity of cellular ATP-generating pathways. The particularly severe ATP depletion in ATCC 13007 may therefore contribute to its lower capacity to sustain ATP-dependent proton extrusion and ion homeostasis under oxygen limitation, helping to explain its greater intracellular acidification and growth inhibition. Conversely, ATCC 9804 maintained ATP levels close to or above the control level even under 50 mM AA, suggesting a greater capacity to preserve energetic homeostasis during severe AA stress.

AA exposure induced marked changes in J_{Na}^+ and J_K^+ fluxes, revealing a substantial reorganization of ion homeostasis. This correlates with the previous studies showing that failure to maintain pH homeostasis has a serious impact on the generation of the proton gradients required for proper potassium transport and distribution [12]. Total J_{Na}^+ increases by 60-110% under 20-50 mM AA stress conditions in *S. cerevisiae* ATCC 9804 and ATCC 13007 strains (Fig. 4). 50 mM AA seriously impairs potassium transport systems in either strain, resulting in relative decline of total and DCCD-sensitive ion flux. Thus, AA stress altered the coordination between Na^+, K^+, and H^+ transport, with the strongest disruption occurring when oxygen limitation was combined with high AA concentration.

Results show (Fig. 5) that exposure of both strains resulted dose-dependent changes in ion flux ratios across the plasma membrane. AA treatment increased the DCCD-sensitive the Na^+/H^+ ratio in both strains under aerobic conditions (Fig. 5A; B) suggesting a strong stimulation of Na^+ efflux coupled with proton transport under acid stress, which was directly proportional ($R^2 = 0.99$) to the increasing AA concentration in *S. cerevisiae* ATCC 9804. This response may serve to counterbalance increased proton influx associated with AA diffusion through cell membrane at medium pH < pK_a. The strong, dose-dependent increase in the DCCD-sensitive Na^+/H^+ ratio demonstrates that Na^+–proton exchange becomes a dominant compensatory mechanism under AA stress, particularly in ATCC 9804 suggesting that Na^+/H^+ exchange contributes to ion and pH homeostasis under AA stress. Nha1 is one candidate transporter that may contribute to this response. This finding is consistent with literature describing Nha1 as a plasma-membrane $Na^+/K^+/H^+$ antiporter involved in maintaining ionic and pH homeostasis under weak-acid stress, while Nhx1 has been implicated in intracellular compartment pH regulation (Table 2) [9,43]. Besides, another Na^+ exporting plasma membrane ATPase, Ena1, is barely translated under acidic pH [9]. However, the mechanisms of Nha1 function during AA stress tolerance are still uncovered and, it's believed, that the role of Nha1 and, especially its relative Nhx1, is the modulation of pH_{in}, by opposing the activity of the V-type H^+-ATPase to alkalinize cellular compartments [57].

Disruptions in K^+ homeostasis can impact on the distribution and balance of other ions and lead to cellular dysfunction: for instance, potassium has been shown to affect copper and iron metabolism [58]. Notably, Trk1, the main potassium influx system in yeast plasma membrane, has been associated with *S. cerevisiae*'s tolerance to AA stress, as demonstrated by the inability of cells lacking this transporter system to grow under these conditions [41]. In addition, Trk1/2-mediated K^+ uptake and Tok1-mediated K^+ efflux have been described as complementary components of membrane-potential and ionic-balance control during acid stress (Table 2) [9]. However, the regulation of Trk1 is complex and has not been characterized under AA stress yet [59]. Here we show that AA reduced the DCCD-sensitive K^+/H^+ ratio, indicating a

progressive impairment of K^+ uptake relative to proton efflux under AA stress. This pattern could reflect altered contributions of K+ uptake and efflux systems, including Trk- and Tok1-mediated transport, although the activities or expression of these individual transporters were not directly measured. The increase in Γ at higher AA concentrations indicates that Na^+ and H^+ efflux became increasingly disproportionate to K^+ uptake, revealing a loss of coordinated ion exchange rather than simply increased proton efflux. This imbalance was more pronounced under oxygen limitation, where ATP availability and membrane organization may constrain the capacity to maintain coordinated transport. The preservation of lower Γ values under moderate stress in ATCC 9804 is therefore consistent with its greater capacity to maintain ionic and pH homeostasis (Fig. 5C; D).

Under oxygen-limited conditions, upon exposure to 50 mM AA, the DCCD-sensitive Na^+/H^+ ratio decreased in *S. cerevisiae* ATCC 9804, suggesting a partial loss of Na^+ efflux efficiency at this AA concentration. Increasing AA imposes a proton stress that nonlinearly uncouples potassium uptake from proton efflux in dose-dependent manner under oxygen-limited conditions, consistent with AA-induced collapse of ion-transport efficiency. Interestingly, DCCD-sensitive K^+/H^+ ratio remained constant in *S. cerevisiae* ATCC 13007 under AA stress (Fig. 5B), suggesting limited capacity or regulation of K^+ uptake under oxygen limitation. Consistent with these changes, the ion exchange balance remained constant under control and 10 mM AA conditions but increased markedly at 20–50 mM AA, with the magnitude of the increase depending on strain and oxygen availability (Fig. 5C and D). Thus, rather than a uniform increase in proton efflux, AA stress induces a redistribution of ion transport efficiency that is both strain- and oxygen-dependent.

Intracellular pH and transmembrane pH gradient measurements were consistent with progressive cytoplasmic acidification accompanying the AA-induced ion-transport imbalance (Fig. 6). A reduction in the transmembrane H^+ gradient is expected to alter the electrochemical driving forces for membrane ion transport [9]. This interpretation is consistent with the previously observed upregulation and activation of Pma1, Vma1 and Na^+/H^+ and K^+ transport systems in response to AA stress under acidic pH (Table 2). Our results showed that 50 mM AA causes the decrease in the intracellular pH up to 5.6, which is lower than earlier observed value in literature [46], showing that 80 mM AA causes decrease of cytosolic pH to 5.7. This can be associated with lower extracellular pH which leads to more AA import in the cells and corresponding intracellular acidification. Notably intracellular pH below 5.2 leads to the loss of viability and metabolic activity in *S. cerevisiae* [46].

The cytoplasmic acidification can associate also to the disruption in proper K^+/H^+ transport systems as indicated by the results from Fig. 5. Thus, earlier research revealed that to maintain balanced membrane potential, *S. cerevisiae* relies on the coordination of potassium uptake and efflux systems and disruption of high-affinity potassium uptake results in plasma membrane hyperpolarization, whereas the absence of potassium efflux systems leads to plasma membrane depolarization [59].

Furthermore, a decrease in transmembrane pH gradient can disrupt membrane transport processes. To our knowledge, no direct experimental measurements of membrane potential ($\Delta\Psi$) at pH 3.0 have been reported. Under standard conditions, the membrane potential of *S. cerevisiae* cells is approximately −170 mV at pH 4.0 [60,61]. Another study reported that decreasing the extracellular pH to 3.0 further reduces the membrane potential [62], resulting in an estimated value of approximately −130 mV. The reduction in ΔpH observed under increasing AA stress is expected to decrease the proton-motive contribution to transmembrane ion transport and may alter the driving forces governing K+ and Na + transport. Although membrane potential was not directly measured in the present study, the observed changes in K+/H+ coupling are consistent with altered electrochemical conditions at the plasma membrane. According to the proton motive force equation, the decrease in the transmembrane pH gradient from ~3.3 to ~2.6 observed in under oxygen-limited conditions (Fig. 6) could lead to an additional membrane depolarization of approximately 40 mV. Altogether, these estimations suggest that exposure to 50 mM AA may depolarize the membrane to approximately −90 mV, a range that may favor Tok1 channel activation and consequently support K^+ efflux [62, 63].

To further quantify intracellular acidification and evaluate cytoplasm buffering capacity of each strain under AA stress, intracellular proton concentration ($[H^+]_{in}$) was calculated from measured pH_{in} values in *S. cerevisiae* ATCC 9804 and ATCC 13007 under aerobic or oxygen-limited conditions (Table 1). Results revealed substantial differences in cytoplasmic acidification between strains, AA concentrations, and oxygen conditions. ATCC 9804 consistently maintained lower intracellular proton accumulation than ATCC 13007 under comparable conditions, particularly during aerobic growth. The absence of a detectable increase in $[H^+]_{in}$ at 10 mM AA in ATCC 9804 correlates with its unchanged growth rate, suggesting effective buffering and proton extrusion capacity. In contrast, ATCC 13007 exhibited significant increases in $[H^+]_{in}$ even at low AA concentrations, indicating limited buffering capacity or higher proton permeability. Oxygen limitation amplified intracellular proton accumulation in both strains.

The intracellular ATP data (Fig. 7) further supports this relationship between energetic status and intracellular pH control. Under oxygen-limited conditions, ATCC 9804 exhibited a pronounced increase in ATP at 10–20 mM AA, whereas ATCC 13007 showed a much smaller response at 10 mM AA and a lower capacity to maintain ATP under severe stress. The dramatic ATP depletion in ATCC 13007 at 50 mM AA coincided with the strongest intracellular acidification and growth inhibition observed under oxygen limitation. Thus, the ability to maintain ATP availability may contribute to sustaining the active proton export or vacuolar accumulation and required to limit cytoplasmatic proton accumulation. Although ATP levels alone cannot establish a causal relationship with intracellular pH regulation, the parallel changes in ATP availability, proton fluxes, and intracellular pH support a close association between cellular energy status and the capacity to maintain pH homeostasis during AA stress.

Thus, in this study, we demonstrate that AA tolerance in *S. cerevisiae* is not solely determined by acid concentration but is fundamentally reshaped by oxygen availability and strain background. By directly quantifying Na^+, K^+, and H^+ fluxes, we show that AA stress induces a strain- and oxygen-dependent reorganization of plasma membrane ion transport rather than a uniform increase in proton efflux. The working model of observed results is presented in Fig. 8. Oxygen limitation stimulates intracellular acidification and disrupts ion flux coordination, leading to non-linear shifts in Na^+/H^+ and K^+/H^+ exchange and a marked increase in ion exchange imbalance that correlates with growth inhibition. Notably, the more tolerant strain, *S. cerevisiae* ATCC 9804, maintains lower intracellular proton accumulation and more efficient ion flux coupling, and a higher capacity to maintain intracellular ATP availability under AA stress, particularly under oxygen-limited conditions. Moderate AA stress was accompanied by increased intracellular ATP, particularly in ATCC 9804 under oxygen limitation, whereas severe AA stress caused ATP depletion, most strongly in ATCC 13007. Together with the ion-flux and pH data, these findings suggest that AA tolerance depends on the capacity to match the energetic cost of ion and proton homeostasis with available ATP-generating capacity. These findings indicate that successful AA adaptation requires not only efficient ion transport and intracellular pH regulation but also sufficient energetic capacity to sustain these processes. The ability of ATCC 9804 to preserve ATP availability under stress may therefore contribute to its superior maintenance of ion and pH homeostasis compared with ATCC 13007.

From an industrial perspective, the results suggest that AA tolerance should be evaluated under oxygen conditions that reproduce the intended fermentation process rather than under a single standardized aeration condition. For lignocellulosic hydrolysate fermentation, strains

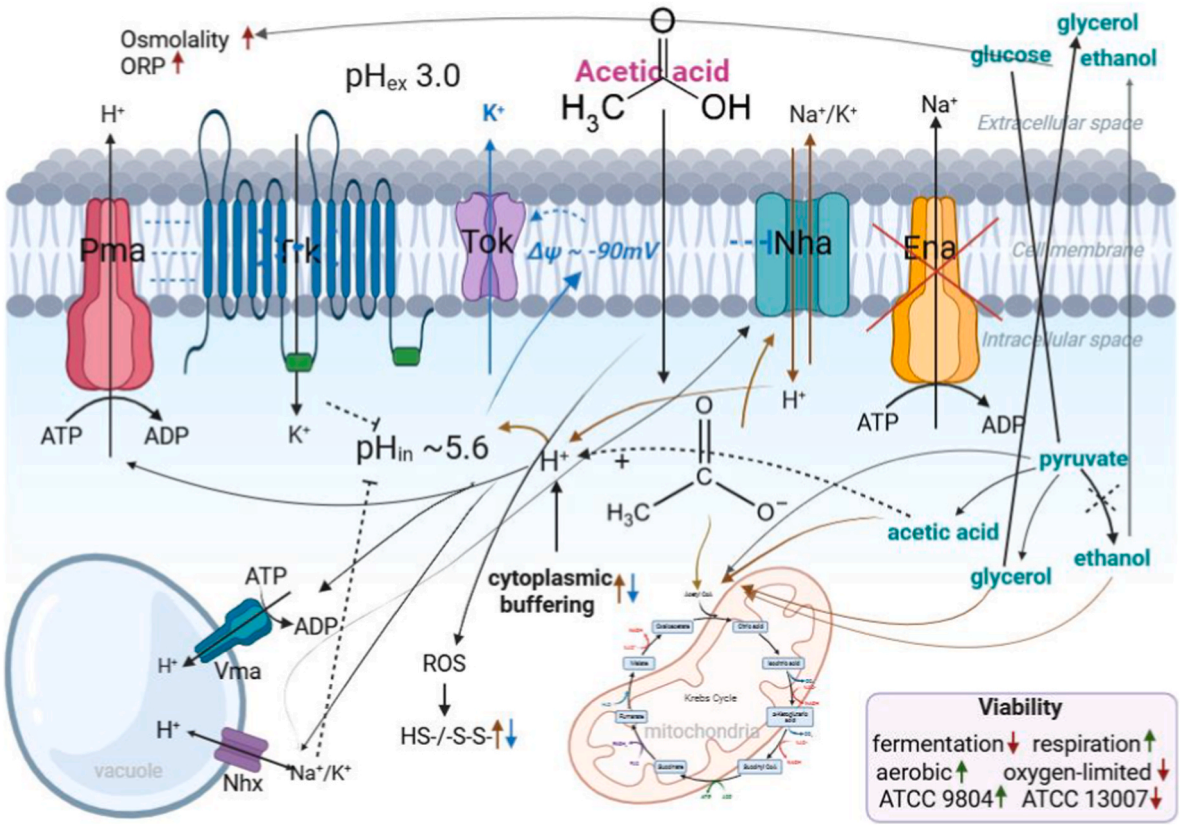


Fig. 8. Working model of *S. cerevisiae* cells response to AA exposure depending on oxygen availability. Abbreviations: Ena - Exitus NAtrii (P-type ATPase Sodium pump); Nha - Na^+/H^+ or K^+/H^+ antiporter; Pma - plasma membrane ATPase; Trk - TRansport of K^+ (Potassium transporter); Tok-target of K1 toxin (voltage-gated potassium efflux channel); Vma-vacuolar membrane ATPase; Nhx-vacuolar Na^+/H^+ or K^+/H^+ antiporter; ORP-oxidation-reduction potential; ATP - adenosine triphosphate; ADP – adenosine diphosphate; Symbols: black symbols-oxygen-independent pathways; brown symbols – aerobic specific pathways; blue symbols – oxygen-limited specific pathways; red-cross-acidic pH-induced inhibition of Ena; blue-cross-partial leakage on membrane or partial inhibition of Trk systems; → stimulate; ⊣ inhibition; ↑ high level; ↑ low level. The model is made by using Biorender.com. (For interpretation of the references to colour in this figure legend, the reader is referred to the Web version of this article.)

such as ATCC 9804-like phenotypes, characterized by preservation of ATP availability, intracellular pH and coordinated $K^+/Na^+/H^+$ transport under oxygen limitation, may represent more suitable candidates for AA-rich substrates. Process development could additionally use controlled oxygen availability during the early growth and stress-adaptation phase to support energy-dependent ion homeostasis, followed by optimization of oxygen supply according to the desired balance between biomass formation, respiration and ethanol production. The ion-exchange balance and intracellular ATP response identified here may therefore serve as physiological screening indicators for selecting strains and defining oxygen-management strategies. These applications require validation in hydrolysates and larger-scale fermentations, where AA concentration, sugar composition and other inhibitors may interact.

CRediT authorship contribution statement

Gohar Azbekyan: Writing – original draft, Methodology, Investigation, Formal analysis. **Anahit Shirvanyan:** Writing – original draft, Methodology, Investigation, Formal analysis, Data curation, Conceptualization. **Nicoletta Guaragnella:** Writing – review & editing, Resources, Investigation, Funding acquisition, Conceptualization. **Rodrigo Ledesma-Amaro:** Writing – review & editing, Resources, Investigation, Funding acquisition, Conceptualization. **Karen Trchounian:** Writing – review & editing, Supervision, Resources, Project administration, Methodology, Funding acquisition, Conceptualization.

Conflict of interests

The authors declare no competing interests.

Acknowledgements

The work was supported by a research grant from the Higher Education and Science Committee of the MESCS RA to KT (23LCG-1F003).

Appendix A. Supplementary data

Supplementary data to this article can be found online at https://doi.org/10.1016/j.abb.2026.111008.

Data availability

Data will be made available on request.

References

[1] S.R. Chaves, A. Rego, V.M. Martins, C. Santos-Pereira, M.J. Sousa, M. Côrte-Real, Regulation of cell death induced by acetic acid in yeasts, Front. Cell Dev. Biol. 9 (2021), https://doi.org/10.3389/fcell.2021.642375.

[2] A. Vilela-Moura, D. Schuller, A. Mendes-Faia, R.D. Silva, S.R. Chaves, M.J. Sousa, M. Côrte-Real, The impact of acetate metabolism on yeast fermentative performance and wine quality: reduction of volatile acidity of grape musts and wines, Appl. Microbiol. Biotechnol. 89 (2011) 271–280, https://doi.org/10.1007/s00253-010-2898-3.

[3] N. Guaragnella, M. Bettiga, Acetic acid stress in budding yeast: from molecular mechanisms to applications, Yeast 38 (2021) 391–400, https://doi.org/10.1002/yea.3651.

[4] R.A. Ribeiro, M.V. Vitorino, C.P. Godinho, N. Bourbon-Melo, T.T. Robalo, F. Fernandes, M.S. Rodrigues, I. Sá-Correia, Yeast adaptive response to acetic acid stress involves structural alterations and increased stiffness of the cell wall, Sci. Rep. 11 (2021) 12652, https://doi.org/10.1038/s41598-021-92069-3.

[5] X. Zhang, J.G. Nijland, A.J.M. Driessen, Combined roles of exporters in acetic acid tolerance in Saccharomyces cerevisiae, Biotechnol. Biofuels Bioprod. 15 (2022) 67, https://doi.org/10.1186/s13068-022-02164-4.

[6] P. Geng, L. Zhang, G.Y. Shi, Omics analysis of acetic acid tolerance in Saccharomyces cerevisiae, World J. Microbiol. Biotechnol. 33 (2017) 94, https://doi.org/10.1007/s11274-017-2259-9.

[7] R.A. Ribeiro, N. Bourbon-Melo, I. Sá-Correia, The cell wall and the response and tolerance to stresses of biotechnological relevance in yeasts, Front. Microbiol. 13 (2022), https://doi.org/10.3389/fmicb.2022.953479.

[8] P.C. Salas-Navarrete, P. Rosas-Santiago, R. Suárez-Rodríguez, A. Martínez, L. Caspeta, Adaptive responses of yeast strains tolerant to acidic pH, acetate, and supraoptimal temperature, Appl. Microbiol. Biotechnol. 107 (2023) 4051–4068, https://doi.org/10.1007/s00253-023-12556-7.

[9] M. Antunes, I. Sá-Correia, The role of ion homeostasis in adaptation and tolerance to acetic acid stress in yeasts, FEMS Yeast Res. 24 (2024), https://doi.org/10.1093/femsyr/foae016.

[10] P. Piper, C.O. Calderon, K. Hatzixanthis, M. Mollapour, Weak acid adaptation: the stress response that confers yeasts with resistance to organic acid food preservatives, Microbiology (N. Y) 147 (2001) 2635–2642, https://doi.org/10.1099/00221287-147-10-2635.

[11] J. Ariño, J. Ramos, H. Sychrová, Alkali metal cation transport and homeostasis in yeasts, Microbiol. Mol. Biol. Rev. 74 (2010) 95–120, https://doi.org/10.1128/MMBR.00042-09.

[12] J. Ariño, J. Ramos, H. Sychrova, Monovalent cation transporters at the plasma membrane in yeasts, Yeast 36 (2019) 177–193, https://doi.org/10.1002/yea.3355.

[13] A. Shirvanyan, K. Trchounian, Sodium transport and redox regulation in Saccharomyces cerevisiae under osmotic stress depending on oxygen availability, Sci. Rep. 14 (2024) 23982, https://doi.org/10.1038/s41598-024-75108-7.

[14] A.L. Waterhouse, G.L. Sacks, D.W. Jeffery, Understanding Wine Chemistry, Wiley, 2016, https://doi.org/10.1002/9781118730720.

[15] G. Fleet, Yeast interactions and wine flavour, Int. J. Food Microbiol. 86 (2003) 11–22, https://doi.org/10.1016/S0168-1605(03)00245-9.

[16] K. Tang, Q. Li, Biochemistry of wine and beer fermentation, in: Current Developments in Biotechnology and Bioengineering, Elsevier, 2017, pp. 281–304, https://doi.org/10.1016/B978-0-444-63666-9.00011-X.

[17] M.B. Pedersen, DNA sequence polymorphisms in the genus saccharomyces III. Restriction endonuclease fragment patterns of chromosomal regions in brewing and other yeast strains, Carlsberg Res. Commun. 51 (1986) 163–183, https://doi.org/10.1007/BF02907322.

[18] M. Hansen, W. Röcken, C.-C. Emeis, Construction of yeast strains for the production of low-carbohydrate beer, J. Inst. Brew. 96 (1990) 125–129, https://doi.org/10.1002/j.2050-0416.1990.tb01022.x.

[19] Z. Zhu, Y. Hu, P.G. Teixeira, R. Pereira, Y. Chen, V. Siewers, J. Nielsen, Multidimensional engineering of Saccharomyces cerevisiae for efficient synthesis of medium-chain fatty acids, Nat. Catal. 3 (2020) 64–74, https://doi.org/10.1038/s41929-019-0409-1.

[20] S. Mirzoyan, A. Trchounian, K. Trchounian, Role of hydrogenases 3 and 4 in Escherichia coli growth and H2 producing hydrogenase activity during anaerobic utilization of lactose, Int. J. Hydrogen Energy 43 (2018) 18151–18159, https://doi.org/10.1016/j.ijhydene.2018.08.032.

[21] L. Yaping, Z. Bo, E. Kalamiyets, W. Peng, C. Jie, Research on response surface optimization of culture medium for antibacterial substances produced by Bacillus amyloliquefaciens GN59, in: Proceedings of the 2019 9th International Conference on Bioscience, Biochemistry and Bioinformatics, ACM, New York, NY, USA, 2019, pp. 75–81, https://doi.org/10.1145/3314367.3314368.

[22] I.K. Olivares-Marin, J.C. González-Hernández, C. Regalado-Gonzalez, L. A. Madrigal-Perez, em>Saccharomyces cerevisiae exponential growth kinetics in batch culture to analyze respiratory and fermentative metabolism, JoVE J. (2018), https://doi.org/10.3791/58192.

[23] S. Sahu, B. Utkalaja, S. Patel, N. Acahrya, Spot Assay and Colony Forming Unit (CFU) Analyses–based sensitivity test for Candida albicans and Saccharomyces cerevisiae</em&gt, Bio. Protoc. 13 (2023), https://doi.org/10.21769/BioProtoc.4872.

[24] K. Son, Y. Shin, D. Il Yoo, Effect of pH condition on natural indigo (Indigofera tinctoria) reduction by yeast (Saccharomyces cerevisiae), Fibers Polym. 20 (2019) 2570–2580, https://doi.org/10.1007/s12221-019-9214-3.

[25] E. Wollmer, F. Karkossa, L. Freerks, A.-E. Hetberg, G. Neal, J. Porter, M. J. Whitaker, D. Margetson, S. Klein, A biopredictive in vitro approach for assessing compatibility of a novel pediatric hydrocortisone drug product within common pediatric dosing vehicles, Pharm. Res. 37 (2020) 203, https://doi.org/10.1007/s11095-020-02912-x.

[26] A. Shirvanyan, S. Mirzoyan, K. Trchounian, Relationship between proton/potassium fluxes and central carbon catabolic pathways in different Saccharomyces cerevisiae strains under osmotic stress conditions, Process Biochem. 133 (2023) 309–318, https://doi.org/10.1016/j.procbio.2023.09.015.

[27] J. Jesus, F. Castro, A. Niemelä, M.-T. Borges, A.S. Danko, Evaluation of the impact of different soil salinization processes on organic and mineral soils, Water Air Soil Pollut. 226 (2015) 102, https://doi.org/10.1007/s11270-015-2373-y.

[28] E.O. Puchkov, I.S. Bulatov, V.P. Zinchenko, Investigation of intracellular pH in *Escherichia coli* by 9-aminoacridine fluorescence measurements, FEMS Microbiol. Lett. 20 (1983) 41–45, https://doi.org/10.1111/j.1574-6968.1983.tb00086.x.

[29] H. Gevorgyan, K. Trchounian, FOF1-ATPase mediates regulation of fermentation and energy metabolism at pH 5.5, Sci. Rep. 15 (2025) 35873, https://doi.org/10.1038/s41598-025-21047-w.

[30] G.K. Sureshkumar, R. Mutharasan, Intracellular pH based controlled cultivation of yeast cells: I. Measurement methodology, Biotechnol. Bioeng. 41 (1993) 118–128, https://doi.org/10.1002/bit.260410116.

[31] S. Sasikumar, S. Taylor Parkins, S. Sudarsan, H. Sinha, Interaction of genetic variants activates latent metabolic pathways in yeast, Nat. Commun. 16 (2025) 8014, https://doi.org/10.1038/s41467-025-63306-4.

[32] M.B. Lemus, J.A. Bayliss, S.H. Lockie, V.V. Santos, A. Reichenbach, R. Stark, Z. B. Andrews, A stereological analysis of NPY, POMC, orexin, GFAP astrocyte, and Iba1 microglia cell number and volume in diet-induced Obese Male mice, Endocrinology 156 (2015) 1701–1713, https://doi.org/10.1210/en.2014-1961.

[33] A. Shirvanyan, A. Primavera, N. Guaragnella, R. Ledesma-Amaro, K. Trchounian, Thiol groups are determinant for overcoming acetic acid and pH stress in wine and beer fermentation-derived *Saccharomyces cerevisiae* strains, FEMS Yeast Res. 26 (2026), https://doi.org/10.1093/femsyr/foag004.

[34] N.P. Mira, M. Palma, J.F. Guerreiro, I. Sá-Correia, Genome-wide identification of Saccharomyces cerevisiae genes required for tolerance to acetic acid, Microb. Cell Fact. 9 (2010) 79, https://doi.org/10.1186/1475-2859-9-79.

[35] M. Mollapour, P.W. Piper, Hog1 mitogen-activated protein kinase phosphorylation targets the yeast Fps1 aquaglyceroporin for endocytosis, thereby rendering cells resistant to acetic acid, Mol. Cell Biol. 27 (2007) 6446–6456, https://doi.org/10.1128/MCB.02205-06.

[36] J. Lee, K. Tatebayashi, D.E. Levin, Acetic acid–induced stress granules function as scaffolding complexes for Hog1 activation by Pbs2, JCB (J. Cell Biol.) 224 (2025), https://doi.org/10.1083/jcb.202409072.

[37] P.-L. Ye, B. Yuan, X.-Q. Wang, M.-M. Zhang, X.-Q. Zhao, Modification of phosphorylation sites in the yeast lysine methyltransferase Set5 exerts influences on the mitogen-activated protein kinase Hog1 under prolonged acetic acid stress, Microbiol. Spectr. 11 (2023), https://doi.org/10.1128/spectrum.03011-22.

[38] N. Baldi, S.C. de Valk, M. Sousa-Silva, M. Casal, I. Soares-Silva, R. Mans, Evolutionary engineering reveals amino acid substitutions in Ato2 and Ato3 that allow improved growth of *Saccharomyces cerevisiae* on lactic acid, FEMS Yeast Res. 21 (2021), https://doi.org/10.1093/femsyr/foab033.

[39] M. Casal, S. Paiva, O. Queirós, I. Soares-Silva, Transport of carboxylic acids in yeasts, FEMS Microbiol. Rev. 32 (2008) 974–994, https://doi.org/10.1111/j.1574-6976.2008.00128.x.

[40] Y. Dong, J. Hu, L. Fan, Q. Chen, RNA-Seq-based transcriptomic and metabolomic analysis reveal stress responses and programmed cell death induced by acetic acid in Saccharomyces cerevisiae, Sci. Rep. 7 (2017) 42659, https://doi.org/10.1038/srep42659.

[41] M.N. Mota, M. Matos, N. Bahri, I. Sá-Correia, Shared and more specific genetic determinants and pathways underlying yeast tolerance to acetic, butyric, and octanoic acids, Microb. Cell Fact. 23 (2024) 71, https://doi.org/10.1186/s12934-024-02309-0.

[42] J.F. Guerreiro, N.P. Mira, A.X.S. Santos, H. Riezman, I. Sá-Correia, Membrane phosphoproteomics of yeast early response to acetic acid: role of Hrk1 kinase and lipid biosynthetic pathways, in particular sphingolipids, Front. Microbiol. 8 (2017), https://doi.org/10.3389/fmicb.2017.01302.

[43] M. Eigenfeld, R. Kerpes, T. Becker, Understanding the impact of industrial stress conditions on replicative aging in Saccharomyces cerevisiae, Frontiers in Fungal Biology 2 (2021), https://doi.org/10.3389/ffunb.2021.665490.

[44] N. Saha, S. Swagatika, R.S. Tomar, Investigation of the acetic acid stress response in Saccharomyces cerevisiae with mutated H3 residues, Microb. Cell 10 (2023) 217–232, https://doi.org/10.15698/mic2023.10.806.

[45] J.D. Duncan, H. Devillers, C. Camarasa, M.E. Setati, B. Divol, Oxygen alters redox cofactor dynamics and induces metabolic shifts in Saccharomyces cerevisiae during alcoholic fermentation, Food Microbiol. 124 (2024) 104624, https://doi.org/10.1016/j.fm.2024.104624.

[46] P.C. Salas-Navarrete, A.I.M. de Oca Miranda, A. Martínez, L. Caspeta, Evolutionary and reverse engineering to increase Saccharomyces cerevisiae tolerance to acetic acid, acidic pH, and high temperature, Appl. Microbiol. Biotechnol. 106 (2022) 383–399, https://doi.org/10.1007/s00253-021-11730-z.

[47] S. Giannattasio, N. Guaragnella, M. Ždralević, E. Marra, Molecular mechanisms of Saccharomyces cerevisiae stress adaptation and programmed cell death in response to acetic acid, Front. Microbiol. 4 (2013), https://doi.org/10.3389/fmicb.2013.00033.

[48] W. Samakkarn, P. Vandecruys, M.R.F. Moreno, J. Thevelein, K. Ratanakhanokchai, N. Soontorngun, New biomarkers underlying acetic acid tolerance in the probiotic yeast Saccharomyces cerevisiae var. boulardii, Appl. Microbiol. Biotechnol. 108 (2024) 153, https://doi.org/10.1007/s00253-023-12946-x.

[49] E. Rozpędowska, L. Hellborg, O.P. Ishchuk, F. Orhan, S. Galafassi, A. Merico, M. Woolfit, C. Compagno, J. Piškur, Parallel evolution of the make–accumulate–consume strategy in Saccharomyces and Dekkera yeasts, Nat. Commun. 2 (2011) 302, https://doi.org/10.1038/ncomms1305.

[50] R. Ke, P.J. Ingram, K. Haynes, An integrative model of ion regulation in yeast, PLoS Comput. Biol. 9 (2013) e1002879, https://doi.org/10.1371/journal.pcbi.1002879.

[51] A. Smidova, K. Stankova, O. Petrvalska, J. Lazar, H. Sychrova, T. Obsil, O. Zimmermannova, V. Obsilova, The activity of Saccharomyces cerevisiae Na+, K+/H+ antiporter Nha1 is negatively regulated by 14-3-3 protein binding at serine 481, Biochim. Biophys. Acta Mol. Cell Res. 1866 (2019) 118534, https://doi.org/10.1016/j.bbamcr.2019.118534.

[52] L. Ferraz, K. Vorauer-Uhl, M. Sauer, M.J. Sousa, P. Branduardi, Impact of ergosterol content on acetic and lactic acids toxicity to *Saccharomyces cerevisiae*, Yeast 40 (2023) 152–165, https://doi.org/10.1002/yea.3828.
[53] R.A. Ribeiro, C.P. Godinho, M.V. Vitorino, T.T. Robalo, F. Fernandes, M. S. Rodrigues, I. Sá-Correia, Crosstalk between yeast cell plasma membrane ergosterol content and cell wall stiffness under acetic acid stress involving Pdr18, J. Fungi 8 (2022) 103, https://doi.org/10.3390/jof8020103.
[54] A. Rego, K.F. Cooper, J. Snider, Y.A. Hannun, V. Costa, M. Côrte-Real, S.R. Chaves, Acetic acid induces Sch9p-dependent translocation of Isc1p from the endoplasmic reticulum into mitochondria, Biochim. Biophys. Acta Mol. Cell Biol. Lipids 1863 (2018) 576–583, https://doi.org/10.1016/j.bbalip.2018.02.008.
[55] Z. Guo, L. Olsson, Physiological responses to acid stress by *Saccharomyces cerevisiae* when applying high initial cell density, FEMS Yeast Res. 16 (2016) fow072, https://doi.org/10.1093/femsyr/fow072.
[56] A. Peetermans, M.R. Foulquié-Moreno, J.M. Thevelein, Mechanisms underlying lactic acid tolerance and its influence on lactic acid production in Saccharomyces cerevisiae, Microb. Cell 8 (2021) 111–130, https://doi.org/10.15698/mic2021.06.751.
[57] C.L. Brett, D.N. Tukaye, S. Mukherjee, R. Rao, The yeast endosomal Na^+ (K^+)/H^+ Exchanger Nhx1 regulates cellular pH to control vesicle trafficking, Mol. Biol. Cell 16 (2005) 1396–1405, https://doi.org/10.1091/mbc.e04-11-0999.
[58] F. Zhang, J. Bian, X. Chen, J. Huang, N. Smith, W. Lu, Y. Xu, J. Lee, X. Wu, Roles for intracellular cation transporters in respiratory growth of yeast, Metallomics 11 (2019) 1667–1678, https://doi.org/10.1039/c9mt00145j.
[59] J. Masaryk, H. Sychrová, Yeast Trk1 potassium transporter gradually changes its affinity in response to both external and internal signals, J. Fungi 8 (2022) 432, https://doi.org/10.3390/jof8050432.
[60] G. Houdinet, C. Guerrero-Galán, B.D. Rose, K. Garcia, S.D. Zimmermann, Secrets of the fungus-specific potassium channel TOK family, Trends Microbiol. 31 (2023) 511–520, https://doi.org/10.1016/j.tim.2022.11.007.
[61] A. Peña, N.S. Sánchez, Y. Ramiro-Cortés, M. Calahorra, Effects of medium pH on the yeast plasma membrane potential, Arch. Biochem. Biophys. 760 (2024) 110131, https://doi.org/10.1016/j.abb.2024.110131.
[62] V. Volkov, Quantitative description of ion transport via plasma membrane of yeast and small cells, Front. Plant Sci. 6 (2015), https://doi.org/10.3389/fpls.2015.00425.
[63] J. Plášek, D. Gášková, J. Ludwig, M. Höfer, Early changes in membrane potential of Saccharomyces cerevisiae induced by varying extracellular K+, Na+ or H+ concentrations, J. Bioenerg. Biomembr. 45 (2013) 561–568, https://doi.org/10.1007/s10863-013-9528-6.